Atmos. Chem. Phys. Discuss.,
https://doi.org/10.5194/acp-2018-1012-RC1, 2018
© Author(s) 2018. This work is distributed under
the Creative Commons Attribution 4.0 License.

Atmospheric Chemistry and Physics Discussions

Interactive comment on "Observations of OH-airglow from ground, aircraft, and satellite: investigation of wave-like structures before a minor stratospheric warming" *by* Sabine Wüst et al.

Anonymous Referee #1

Received and published: 29 December 2018

We would like to thank the anonymous referee for his valuable comments. We answered all of them and changed the manuscript accordingly. Please find the details below in orange.

General comments:

This manuscript describes and analyzes observations of OH airglow emissions from different platforms (particularly from the FALCON aircraft) during a field campaign in Scandinavia in January 2016. The paper is in general well written and easy to fol-

Printer-friendly version

Discussion paper

low. Although it does not provide any really new insights into the topic, the manuscript should in my opinion by published. It will probably be complemented by other publications dealing with the same field campaign. I recommend accepting the manuscript subject to minor revisions. Below I offer some (mainly really minor) suggestions for improvements.

Specific comments:
Page 1, line 29: 'emphasize' -> 'emphasis' Done

Page 2, line 12: 'mounted at' -> 'mounted on' ? I think that's right, I changed it also in section 2.2

Page 2, line 14: 'all other airborne measurements address heights of ca. 20 km and below.'

It's not entirely clear, what this part of the sentence refers to? To other instrumentation on Falcon? Yes, I added this information.

Page 3, line 25: I suggest replacing 'x' in '320 px x 256 px' by ' times' (I assume you use LaTex?) I use Word, but I think I found the sign you meant in the formula editor, I substituted "x" when it was used in the sense of "times" in the whole manuscript

Page 3, line 30: '(compare Fig. 7 and 10).'

not sure, how this can be seen in Figures 7 and 10? Do the arrows indicate the flight track? Yes they do, I added this info in the caption. The observed area is sometimes left, sometimes right of the arrows. Yes, we put the arrows where we thought there is enough space and where it fits best. But we can change it if you like.

Page 4, line 22: 'and upper levels'

It's not entirely clear, what 'upper levels' refers to. It may refer to 'upper atmospheric levels'or 'levels of excitation'. It's most likely the latter. Please specify. I mean higher altitude levels and added this information

Page 4, line 24: delete comma before '1.04 and 1.06' Done

CC BY

Page 4, lines 28 – 30: Perhaps a paper on the validation of SABER temperature observations can be cited here? … Done (Dawkins, E. C. M., Feofilov, A., Rezac, L., Kutepov, A. A., Janches, D., Höffner, J., Chu. X., Lu, X., Mlynczak, M. G., and J. Russell III: Validation of SABER v2.0 operational temperature data with ground-based lidars in the mesosphere-lower thermosphere region (75–105 km). J. Geophys. Res.: Atmos., 123, 9916–9934. 10.1029/2018JD028742, 2018.)

Page 6, line 19: 'information are' -> 'information is' Done

Page 6, line 23: 'the height of 84 km'

Is this the height of maximum VER or a weighted, i.e. centroid altitude?
In this case it is the height of maximum VER, I added this info in the manuscript.

Figure 3: It would be good to mention explicitly in the Caption of Figure 3 that the year 2016 is shown. Done

Page 8, lines 24/25: 'information .. are' -> 'information .. is' Done

Page 9, line 7: 'flight legs parallel'

Perhaps add, e.g. 'roughly' or 'more or less', because the flight legs do not appear to be exactly parallel to the latitude/longitude circle? Done

Caption Figure 7: What exactly do you mean with 'Difference images'? This is later explained in the main text - as I found out - but perhaps it can be explained briefly in the caption, too? Done

Page 11, line 15: 'as well as height and intensity are anticorrelated.'

Regarding the anti-correlation between intensity and emission altitude the papers by Grygalashvyly (2014) and von Savigny (2015) may be cited, too. The first one provides a theoretical explanation for this anticorrelation and the second one shows the relationship for the OH(3-1) band (if I remember correctly), which is of importance to your work.

Grygalashvyly, M., G. R. Sonnemann, F.-J. Lübken, P. Hartogh, and U. Berger (2014), Hydroxyl layer: Mean state and trends at midlatitudes, J. Geophys. Res. Atmos., 119,

CC BY

12,391–12,419, doi:10.1002/ 2014JD022094.

von Savigny, C., Variability of OH(3-1) emission altitude from 2003 to 2011: Long-term stability and universality of the emission rate - altitude relationship, J. Atmos. Sol.-Terr. Physics, 127, 2015.

Done

Page 13, line 19: 'So, if the vertical movements of atomic oxygen are due to a wave, one can conclude that the wave-induced vertical temperature gradient becomes zero where the brightness is maximal or minimal,'

I don't really understand this argument. Please explain.

I try it. Where the airglow brightness is maximal I should have maximal downward movement, where it is minimal I should have maximal upward movement.

When imagining gravity waves as only vertically oscillating coupled air parcels (and neglecting the horizontal component to make it easier), the vertical temperature profile will show a sine. The wave-induced temperature should be maximal where the air parcels are in their lowest position with respect to their rest position (they are deflected maximal downward from their rest position) and minimal when they are in their highest position with respect to their rest position (they are deflected maximal upward from their rest position). In the extreme points of the vertical profile of the temperature fluctuations, the vertical temperature gradient is zero and the brightness should be maximal or minimal.

Caption Figure 8: 'The horizontal line marks the wavelength of 15 km.' There are different horizontal lines. Please specify. I am sorry, the thicker lines moved through the image. I corrected the figure, now, only two lines are visible. This also holds for figure 11.

Interactive comment on Atmos. Chem. Phys. Discuss., https://doi.org/10.5194/acp-2018-1012, 2018.

CC BY

Atmos. Chem. Phys. Discuss.,
https://doi.org/10.5194/acp-2018-1012-RC2, 2019
© Author(s) 2019. This work is distributed under
the Creative Commons Attribution 4.0 License.

Atmospheric Chemistry and Physics Discussions

Interactive comment on "Observations of OH-airglow from ground, aircraft, and satellite: investigation of wave-like structures before a minor stratospheric warming" *by* Sabine Wüst et al.

Anonymous Referee #2

Received and published: 3 January 2019

We would like to thank the anonymous referee for his valuable comments. We answered all of them and changed the manuscript accordingly. Please find the details below in orange.

General Comments The authors present a selection of results from a campaign of observations on OH-airglow emissions recorded from the ground, and from an aircraft flown inside the Arctic Circle during January and February 2016. The ground-based observations were made using infrared spectrometers deployed at ALOMAR and Kiruna, while the aircraft measurements were made with a "Fast" airglow imager taken over

Printer-friendly version

Discussion paper

flight paths that included both observing stations.

These observations were supplemented with the inclusion of temperature and OH* VER profiles from the TIMED-SABER satellite instrument near the time and location of the observations, in addition to horizontal and meridional wind data from the ECMWF.

The SABER data have been used to calculate the mean height and thickness of the OH* layer during the period of the observing campaign. There is good correspondence between the variation of the OH* layer brightness measured by the ground based spectrometers and that obtained from the SABER VER measurements. The Brunt-Väisälä (BV) frequency during the observing campaign was calculated for the OH* layer by weighting it by the VER measurements. It showed a steady decrease throughout the observing period – which was interpreted to imply a reduction in the static stability of the atmosphere during that tim interval.

Combining the OH*-layer averaged temperature data from the infrared spectrometers with the SABER temperature profiles, enabled the authors to calculate the gravity wave potential energy density (GWPED) contained in the spectrometer temperatures. Results were separated into those with periods > 60 and <= 60 minutes. GWPED for waves with T < 60 min were in the range 7 - 15 J/kg, whereas those waves with T > 60 mins were in the range 10 - 150 J/kg. A relatively clear maximum in the GWPED for the former group occurred around January 27th, which is close to the time of a minor stratospheric warming event. The authors interpret this coincidence as possible evidence that these longer period waves originate at tropospheric altitudes. The cubic spine fitted to the two wave groups is of doubtful value.

Images from the FAIM camera were used to calculate wavelengths and propagation directions of the waves and ripples detected in the images. These were separated into those with lambda > 15 km and those <= 15 km. In the case of flight 1 (Kiruna – Alomar and back making a triangle) waves with lambda > 15 were either NW or SE, whereas those with lambda <= 15 km tended to be SW or NE. The highest occurrence rate of waves occurred in both legs when the plane was passing over the highest mountain peaks.

The manuscript is well organised and the data is clearly presented. The methods used

CC BY

to identify the gravity waves in the image sequences are correct and the description of the methods used are clear. The text includes an appropriate set of references. The work is suitable for publication in ACP, provided that the minor points highlighted in the specific comments and in the technical corrections below are addressed.

Specific Comments

On page13, the authors attempt to use the airglow brightness images to deduce something about whether static and dynamic instability is the dominant mechanism generating the ripples in flight 1 or flight 5. This is an interesting idea, but it is based entirely on assumptions which may or may not be true. In the absence of horizontal wind and temperatures data (see page 12, lines 31-33), we cannot say. This passage also assumes a relation between airglow brightness and temperature, which does not always hold strictly as pointed out in lines 17-19 on page 13. Yes, that's true but as reviewer 3 pointed out, at least during this time of the year this assumption holds on average (Garcia-Comas et al., 2017; Shepherd et al., 2006). I integrated this information in the manuscript. I also pointed out the assumptions and used wind measurements at ALOMAR (Stober et al. 2017) in order to motivate at least the argumentation.

A really useful reference on this point is the recent paper by Li et al. (2017), in which the authors study statistically the relation between ripples and the background atmosphere. Some of the statements made in the current manuscript are not supported in the work by Li et al. (2017), e.g., line 30 on page 11 states (referring to ripples) "They move with the background wind . . .". Li et al. (2017) report that less than half of the ripples examined moved with the background wind, and were in fact real wave structures that are difficult to distinguish from real instability features.

The authors should read Li et al. (2017) and revise the current manuscript in the light of the results presented there.

Thank you very much for bringing this paper to my mind. I revised abstract, discussion

CC BY

section and summary accordingly

Technical corrections

It seems to me that some of the technical corrections refer to the manuscript before it was improved during the quick review process. In this case I only mention "already corrected" as answer to the comment.

Page 1, line 27; "evolvement" –> "evolution". Already corrected

Page 1, line 29; "Special emphasize is put . . ." –> "Special emphasis is placed . . .". Done

Page 2, line 29; insert "(BV)" after "Brunt-Väisälä". Done

Page 3, line 18; insert "(GWPED)" after "density". Done

Page 3, line 24; omit "of" in "on board of the DLR". Done

Page 4, line 22; omit "certainly". Done, additionally I think it must be "are" instead of "is" just before the (now-deleted) "certainly"

Page 6, line 10; replace "looked up" by "found". Done

Page 6, line 18; insert " for the calculation of N" after "necessary". Done

Page 6, line 24; "catches" –> "includes". Done

Page 7, line 8; replace "The used 2D FFT algorithm needs equidistant data." by "The 2D FFT algorithm employed requires equidistant data.". Done

Page 9, line 21; insert ";" after "also. Already corrected

Page 9, line 28; "cut" –> "reduced". Done

Page 11, line 15; year of reference (2009) is inconsistent with line 7 on page 17. Already corrected

Page 12, line 17-18; suggest "Therefore, we conclude that gravity waves with periods longer than 60 min are more likely to could to a larger part be generated in the

CC BY

troposphere than gravity waves with periods shorter than 60 min." Done

Page 14, line 7; "In the same time" –> "At the same time". Already corrected

Page 14, line 10; "could not be observed." –> "were not observed." Done

Page 17, lines 5-7; year of reference (1995) is inconsistent with line 15 on page 11. Already corrected

Page 20, line 10; "preceding" –> "subsequent". Already corrected

Page 21, line 6; "stand for" –> represent. Already corrected

Page 24, Figure 6(a) and 6(b); dashed grey line is very faint. Use a darker colour. Already corrected during the quick review. Is it still too faint?

Page 26, Figure 8(a); the grey line that shows the orography is so faint that it is almost impossible to see it. Already corrected during the quick review. Is it still too faint?

Page 29, Figure 11(a); the grey line that shows the orography is so faint that it is almost impossible to see it. Already corrected during the quick review. Is it still too faint?

References Li, J., T. Li, X. Dou, X. Fang, B. Cao, C.-Y. She, T. Nakamura, A. Manson, C. Meek, and D. Thorsen (2017), Characterstics of ripple structures revealed in OH airglow images. J. Geophys. Res. Space Physics, 122, 3748-3759, doi:10.1002/2016JA023538

Interactive comment on Atmos. Chem. Phys. Discuss., https://doi.org/10.5194/acp-2018-1012, 2018.

Printer-friendly version

Discussion paper

Review of "Observations of OH-airglow from ground, aircraft, and satellite: investigation of wave-like structures before a minor stratospheric warming" by Wüst et al. (acp-2018--2012)

We would like to thank the anonymous referee for his valuable comments. We answered all of them and changed the manuscript accordingly. Please find the details below in orange.
Since answers to some comments (e.g. referring to the shaking of the airplane, the range of the different angles, the difference images, …) might be easier to follow we additionally deliver two videos, one for each flight as supplemental material. The left part shows the original image, the mid part shows the flight route colour-coded is the intensity averaged over the respective picture, and the right part shows the difference images.

The authors study pre-SSW gravity waves from airglow and/or temperature measurements in early 2016 using measurements of four different instruments: SABER-TIMED space radiometer, GRIPS9 (Kiruna) and GRIPS14 (Alomar) ground-based spectrometers, and FAIM imager (onboard FALCON aircraft). Following the work in Wüst et al. (2016), the authors derive time variation of BV frequency at the OH layer from SABER and, in combination with GRIPS temperatures, gravity wave potential energy density. They also derived short-time series of GW spectra and propagation direction, and their time variations from two FAIM flights (one of them right before a minor SSW). They detect highest GW occurrence over mountains. They also found dominance of small-scale GW contribution a couple of weeks before the SSW, which was not the case just before the SSW. Leaning on SABER-GRIPS BV frequency evolution and ECMWF data, they concluded that the small-scale waves in the first case were due to convective instability whereas they were due to dynamical instability in the second case. They also conclude that short period waves are generated in the higher stratosphere and above.

The paper is well written and organized, although some explanations could be simpler (particularly in the discussion). The English is ok.

I recommend the manuscript for publication, once the following suggestions and comments are taken into account.

General comments

The introduction does not include a description of previous results and the state-of-the-art in the field of GWs, in particular, before or during SSWs. Also, there is not a description of the scientific interest of the results presented here. Something similar happens in the discussion, which is not put into context of results from other authors or measurements. Indeed, there are previous publications (particularly regarding large scale features) that are not mentioned here. We included references in the manuscript. Since the focus of this paper is on smaller-scale features, we choose the references accordingly. We also included a short description of the scientific interest.

The authors make use of measurements of several variables from 4 different instruments. In several places in the text, it is hard to know the instrument they are referring to or the calculations they are using. That makes the reading slow. For example, Sect. 4.2.1 shows calculations of GWPED that need from GRIPS temperature anomalies and periods, but these and their estimation are not shown nor even discussed anywhere. This happens more often (see comments below) and I recommend the authors reading the manuscript carefully with this criticism in mind in order to address this issue.
We tried to make clearer which results are based on which instrument and also included a description of the GWPED derivation in the analysis section. In order not to lose focus and since the algorithm was published and discussed in detail in Wüst et al. (2016), we kept the description short.

GRIPS14, observing over Alomar, is not used in the analysis. Only its 15-day mean temperatures and intensities are plotted but they are not further analyzed nor used for the discussion. Some information on wave propagation direction could be extracted when combining GRIPS9 (at Kiruna) with GRIPS14 (as in Wüst et al., 2018), perhaps also in the context of FAIM measurements. In any case, the results from GRIPS14 could support (or not) those from GRIPS9 and should be analyzed in parallel here. Additionally, they start early in January and can extend the time series longer.
GRIPS 14 at ALOMAR is not used for the derivation of GW information since the weather situation at ALOMAR was not suitable during the time period when GRIPS 9 measured at Kiruna. This was mentioned in section 2.1 but we now additionally included this info in section 4.2.1 where the GWPED from Kiruna is shown.

In the discussion section, the author's conclusions are more a consistency with the behavior expected. For example, Flight 1 is just consistent with dynamical instability as the origin for ripples and Flight 5, right before the SSW, is not. This subtle difference is important because there is not an examination of other possible sources or very strong evidence from these results behind that idea (on the one hand, it is based on the assumption that changes in brightness are only due to the generating GW; on the other hand, they only have two 2 days of measurements). That should be clear in the text.
We tried to make it clear.

Detailed comments

P2Sect.1. The introduction should be revised. The research is not put into context and the scientific scope of the paper needs to be better described. Just studying gravity waves is not an argument for a scientific paper. Please, include an explanation of the scientific interest. Done
P1. L18-24. Provide a small introduction of FAIM. I assume it's page 2 not page 1. Inserted one sentence.
P1L20. Small-scales, write how small. Done
P1L21. Smaller aperture. How smaller? Done
P2.Sect.2: The instruments are poorly described. It is not easy to understand what and how exactly they measure. Since the focus of this publication is not the instruments, which are described in detail in separate publications, I extended these subsections to some extent (GRIPS more, FAIM less).
Sect. 2.1: Unless you know GRIPS before reading this paper, it is not easy to know how exactly the instrument measures airglow. It is not even clear here that GRIPS is not an imager. What is the spectral resolution? Perhaps describing it here with more detail would help. Done.
P3L7. Are these noise or systematic errors? Include a description of major sources of uncertainty. Done
P3L7. Include reference for temperature retrievals. Done
P3L11 Write observation angles for the 4 FoVs for GRIPS 9 Done
P3L19. Shortly describe how you derive temperatures. Provide errors and error sources. Done.
P3L25. Write the OH transitions this instrument is sensitive to. Done
P3L31. Please, indicate range. Done, yaw angle removed since it only changes the orientation of the FoV.
P4L10. It is not clear. Are they analyzed or not? No, they are not, I changed the sentence to "Therefore, these measurements are not part of this publication." too make it clear.
P4L20. SABER is described in many papers. Better a reference to one of those than to a webpage that may eventually stop working. Sentence deleted
P4L28. Remsberg et al. compared SABER v1.07 temperatures but you are using v2.0. Provide biases for v2.0, wether indicating v1.07-v2.0 comparisons or comparisons of v2.0 with other space and ground based instruments, which are already available. Done
P4L28-32. The authors are mixing here noise and systematic errors. Comparisons with other instruments should be commented in the context of systematic errors. SABER MLT temperature main errors are due to atomic oxygen uncertainties (Remsberg et al. 2008; Garcia-

-Comas et al. 2008). Also the biases strongly depend on latitude. Information concerning the quality of v1.07 deleted and replaced with information concerning v2.0.
P4L32. For coherence, shortly comment on OH VER uncertainties. I found detailed info about the different temperature errors, but I found no publication where this info is provided for the VER.
P5L7. What do you mean by 500m negligible compared to 2000m FWHM? Please, quantify. Done Also note that SABER vertical sampling is several times smaller than its FOV. Done
P6L7. Insert 'Brünt-Vaisala (BV)' Already introduced on page 5
P6L10. One really needs Wüst et al. 2016 in one hand when reading this manuscript, which is not useful. Please, shortly describe why shorter and longer than 60 min. Done
P6L23. For what transition? Done
P7L6. Could you better explain why airplane shaking prevents deriving period and phase speed? What is the error in the wavelength due to this shaking?
The shaking translates the FoV by several pixels in a quasi-periodic manner and applies a motion blur on the images. The translation does not allow deriving the change of phase from consecutive images, but this information is crucial for calculating phase speed and period of the waves. The translation affects the whole image and therefore all wave crests within the image, the wavelength which is derived for each image individually is not influenced. The motion blur does not change the position of the wave crests, but it reduces the amplitude of the waves. The amplitude, however, is not used here. Info added in the text.
P7L8: Delete 'used' Done
P7L15: Please, clarify why you use here 87km and you mention 84km in previous section.
We took 87 km since this is the "standard height" for the OH-airglow layer. A publication which is often cited here is Baker and Stair (1988). We clarified in the previous section that the value 84 km holds only for the time period analysed in Wüst et al., 2016 and that other values are possible. Furthermore, 84 km is the height of maximum VER, the centroid height is mostly slightly higher.
P7L15: Please, quantify the effects of layer altitude. +/-5 km in the altitude layer corresponds to +/-6% in the resolution and therefore also in the wavelength (calculated for a zenith angle of 5°), info added.
P7L19. Please, show in Fig. 1 the resulting image after applying this filter. Done, we additionally show a second example. Here it becomes clear why we choose a square of 26 km x 26 km for the analysis.
P8L4. According to what instrument? SABER, info added
P8L8. starts to rise by -> rises Done
P8L8. varies -> oscillates Done
P8L9. layer altitude Done
P8Sect.4.1. Fig. 2 is full of interesting things. I recommend including a more detail description of the figure here. Taking into account your comment on this figure at the end of the manuscript (Fig. 2. Please, change color code. It is not possible to differentiate most of them from others), I tried different versions but in every case the figure is either not readable for people who are "red-green blind" or the figure becomes confusing (when using different line styles, for example). The main purpose of this figure is to show the behavior of winter 2015/16 compared to the mean over all years. I agree with you that there are certainly many interesting things to deduce concerning the other years, however, I would like to keep the paper focused. Therefore, I decided to delete all curves but the mean and the one referring to winter 2015/16.
P8L10. What SABER intensity is compared here? Averaged over the layer? Peak intensity? Does this choice make a difference? It's the peak intensity (added info in the manuscript) and the choice makes no difference concerning the variations. I calculated the integrated intensities and compared them to the peak intensities. They correlate linearly with an R^2 of about 87%. Info added in the manuscript.
P8L11. Only SABER and ALOMAR show a 4-6 day pronounced periodicity. GRIPS-9 periodicity is 9 days (one should not assume measurement for 15Feb is a maximum.
Changed to "In particular, they show pronounced periodicities in the range of some days". In order to avoid misunderstandings, I would like to mention that figure 4 does not include February, 15th, it ends at the beginning of February. I added this information in the figure caption to make it clear.

P8L12. Not in GRIPS 14. Here, we disagree. Could please have a second look at the figure taking into account the information about the x-axis I gave one comment above?
P8L13. Include SABER OH*-temperatures. If comparable, that would somehow justify the use of SABER BV frequencies. Done. By preparing the new figure, we realized two things: a) we originally used SABER data around Kiruna and not around Alomar; that is a contradiction to section 2.3 where we say that we use only SABER data around Alomar. b) There was a slight offset in the relative GRIPS intensities for Alomar. We corrected both.
P8L18. Please, perform the same analysis with GRIPS 12 since it has a longer time coverage and also, if combined with GRIPS9, some information on horizontal propagation could be extracted. Sorry, but I don't know which analysis you mean. You probably refer the GWPED. As mentioned above the weather at ALOMAR was bad when it was good at Kiruna (bad and good with respect to the derivation of GWPED)
P8L20. Describe here the temperature anomalies (amplitudes) you are using and how you estimated them. I think this information should be mentioned in section 3.1 where the analysis is described.
P8L20. GRIPS temperature amplitudes Can you please concretize your comment?
P8L21. There is no dashed line in Fig. 5 Sorry, it's solid.
P8L22. Include 15-day averages in plot and discuss here in terms of fluctuations around the linear fit. Can you please concretize why you would like to see a 15-day average here and a discussion of the fluctuations around the linear fit? With this figure I intend to show that the BV-frequency decreases overall even though it shows superimposed fluctuations. For the GWPED density I use the exact BV-values and not the linearly fitted ones. I would like to avoid confusing the reader with too many details which are not really necessary for the publication.
P8L24. Shortly describe criteria here. Done
P9L8 principal --> principle Corrected
P9L12. I guess that the authors mean an image horizontal coverage instead of spatial resolution, in contrast to the FoV used in this manuscript to refer to the spatial resolution for GRIPS. Please, homogeneize definitions. Sorry, but I do not understand this comment. We don't say anything about the spatial resolution in this line. Furthermore, this section refers to FAIM as mentioned at the beginning of the section.
P8L14. ... and it also varies with OH layer altitude. You probably mean page 9. Yes, that's true, but the change of the roll (in the following figure denoted as zenith angle) and pitch

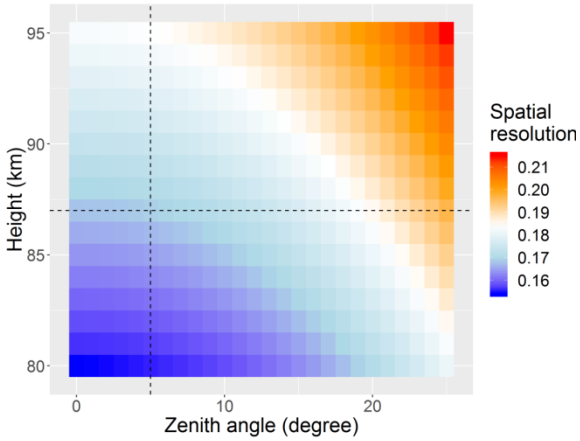

angles dominates possible variations in the OH-layer height during one flight. The roll angle is 25° at maximum.

P9L15. What do you mean by time difference images? Explain how you treat several images overlapping. A difference image is derived by subtracting the intensity measured by each pixel from the intensity measured 10 s later by the same pixel. For this method, it is not a problem, if several images overlap.
P9L27. in sensitive --> is sensitive Corrected
P9L28. Why is the horizontal coverage cut to 26x26? This is the largest square size which does not contain any pixels outside the un-warped image region (marked in Fig. 1). This information is already given in section 3.2, therefore, I don't insert it here.
P9L30. What do you mean by 'small-scale' here? Wavelengths in the range of 15 km and less, info added in the text.
P9L31. But the wavelengths smaller than 15km (1/k = [1/0.1,1/0.15]) appear very

strongly at 17:40–17:55. Don't they? Yes they do, that's why we mentioned the time period 17:30–18:00 in the text.
P10L12–13. This info is not accurate, not used, not analyzed. The reader may loose attention to the central point of the FFT analysis. Deleted
P10L16. What do you mean by this? What do you think it is causing this large mean intensity? See answer to next comment
P10L16. What do you mean by saying this? This is just a result. We interpret it later in section 5. What do you think it is causing this large intensity? That's a good question which we cannot answer based on our measurements. The maximum is comparable in its height to the one in leg 2. The horizontal distance between both maxima does not contradict the assumption of gravity waves (which we make in section 5). For previous flight, you just mentioned that mean intensity changed too much for long wavelenghts analysis....
For the previous flight, we mentioned "The airglow brightness averaged over each picture shows local maxima during these three time periods (Fig. 8a)." The time periods we here refer to are the ones with "high Fourier amplitudes also in the range of small-scale features".
P10L16 maximal –> maximum In this line there exists two times the word "maximal" and after consultation of a dictionary I think one can use this word in both cases.
P11Sect.5. The discussion gets complicated in some paragraphs. Please, re–read and simplify (this specially holds for reasoning in pages 12–13). I re-arranged this section and hope that it became clearer.
P11L3. A better description of the event, including dates of SSW onset and polar vortex displacement and recovery would be more useful. Done
P11L3. Delete 'the' before 'January' Corrected
P11L6–7. Include reference. Done
P11L12. Better than 'neglecting the effect of planetary waves' (which are the responsible for the polar vortex displacement mentioned above', you could write 'We expect the following effect on the zonal means. Corrected
P11L15. Mulligan et al. is missing in the reference list. Already corrected in a former version Grygalashvyly (2015) and Garcia–Comas et al. (2017) should be included in this list. Done
P11L16. Explain why height and thickness are not anticorrelated in Fig 3.
The FWHM was calculated straight forward: the VER-maximum is searched between 70 km and 100 km. 50% of this maximum is calculated. Then, the maximal and minimal height, where the VER is greater than 50% of the VER-maximum is derived. The minimal height is subtracted from the maximal height and this value is denoted as the FWHM. I checked the profiles and the values make sense.
The VER-profile is to some part influenced by oscillations. Depending on the strength of the oscillations, this also influences the FWHM. The anti-correlation reported in literature is observed in a statistical sense. These might be two reasons why figure 3 looks different than expected. However, from the 15-day average shown figure 2 it becomes clear that overall the behavior of the OH*-height and the FHWM is not so far away from what we expect.
P11L17. Insert 'According to SABER measurements,' Done
P11L18. also and particularly during February 2016 (see Fig. 2 and 3). Information added
P12L3. vertical –> horizontal I reformulated this sentence in order to avoid confusion.
P12L10–11. This may confuse the reader. Better saying "winds in the upper stratosphere were stronger than in the upper troposphere" Corrected
P12L11. was –> were Corrected
P12L11. Easterly winds became weaker after Jan 23rd, which, for a continuous source of GWs, should have resulted in less overall filtering and more (E) GWs propagating to the mesosphere until Jan 28th. Yes that's true and agrees with our argumentation. We included the info about the date of wind speed weakening.
I can only glimpse the corresponding response in potential energy density for T<60min but the enhancement on the 27th is clear. Please, discuss on that.
Do you really mean T<60 min? I see the enhancement only for T>60 min. For T<60 min we can speculate about a maximum at Jan. 26th at least compared to mid January (18th) and end of January (28th). I included this info.
Perhaps, analysis of the next days in GRIPS9 time series (until Feb 2nd, as in Fig.4) could

help.
For figure 4, nightly mean temperatures are used. The quality criteria for deriving GWPED are higher. Unfortunately, the data quality of the ALOMAR measurements was relatively bad at the end of January, so further GPWED values cannot be derived.
On the other hand, the change in FAIM total number of wave events before (Fig.9) and at the onset of the SSW (Fig. 12) does not clearly show any difference. Discuss on that also.
The number of wave events changes: it becomes larger by a factor of ca. 1.5–2.0 (for wavelengths shorter or longer than 15 km). We included this information in fig. 9 and 12 as well as in the results and discussion section.
P12, L17. Insert 'according to GRIPS9 data,' after 'Therefore' Done
P12L18. This is too much of a conclusion based on zonal mean winds. Note the potential longitudinal variations or the length of the time series in Fig. 6. That's a misunderstanding; figure 14 does not show zonal means it depicts the wind profile for the grid point next to Kiruna. We additionally inserted a discussion of the meridional component:
"The meridional wind component evolves differently (Fig. 14 b) compared to the zonal one: the direction of the meridional wind varies over the whole height range between January 20th and 27th, 2019. Afterwards, this is not the case any more. If gravity wave filtering is driven by the meridional wind, one expects also in this case that the activity of gravity waves generated in the troposphere increases at the end of January."
P12L19 had the best chance --> had best chance Corrected
P12L21. Again, you should be careful when using zonal means from Fig. 14. I do not think you can resolve measurements over Kiruna using that information alone. That's a misunderstanding, figure 14 does not show zonal means, it shows the wind profile for the grid point next to Kiruna.
P12L25 Please, rewrite sentence Reformulated by taking also into account the next comment.
P12L26. I do not agree that the wind profile is rather flat before Jan 31st. There is a wind reversal around the stratopause and in the troposphere. Reformulated
What can be inferred from GRIPS14 measurements?
As mentioned above, GRIPS 14 measurements at ALOMAR are of insufficient quality for the calculation of GWPED (bad weather).
P12-13 The conclusions the authors reach are not put into context of results from other authors here, in particular, those regarding larger scale features (e.g., Gerrard et al., 2011). Done
P13L2. Insert '(see Fig. 5)' Done
P13L3. What 'airglow brightness maps'? The use of the word "maps" is irritating, we mean information about the airglow brightness → corrected
P13L2. 'Since the measurements were taken in winter' I assume that you refer to line 5. There, I corrected it but in line 2 I don't know what to change.
P13L6. What do you mean by 'overall' here? Note that you may eventually have inversion layers. I changed the sentence to "Thus, as long as inversion layers do not exist, the vertical background temperature gradient is negative in the height range of the OH* layer. Static instability is therefore possible and independent of the existence of gravity waves."
P13L8. Explain here what you define as the 'grey regions' of an airglow image
Done
P13L7: Insert 'According to ECMWF data,' Do you really mean line 7? This line does not refer to ECMWF data
P13L19. Please, make it clear that a correlation does not always hold (as in Pautet et al.) but, on average, a positive correlation between brightness and temperature should be a fair assumption, at least from mid-autumn to mid-winter. This was shown by WINDII and SATIs (Shepherd et al., 2006) but also by SABER, instrument that you use (Garcia-Comas et al., 2017). Thank you for this hint. We included it.
P13L21. Why does the temperature gradient become zero? That depends on the amplitude of the wave. Better saying 'becomes maximum'. In this part, we speak about the wave-induced temperature deviations from the atmospheric background, so we neglect the background. In regions of maximal or minimal wave-induced temperature, the air parcels are deflected maximal from their original position (rest position), so the vertical transport should be maximal there. In regions of maximal or minimal temperature, the temperature gradient is zero.

P13L21. The use of 'steepest' here leads to misunderstanding. Better saying 'the minimum (or, since it is negative, maximum in absolute value) temperature gradient' See answer to comment above, in the regions where the wave has its zero-crossing, the temperature does not change and the gradient is steepest.
P13L23. 'compared to' --> 'depending on' Sentence deleted, it probably causes more confusion than it helps.
P13L25. Do you mean the 'zonal wind shear' yes and info added
P13L27. Could you be more precise and describe the bright airglow areas you are referring to? Legs 4 and 5? Done
How do you know these small-scale structures are only caused by a larger dynamical instability instead of any other cause, like location or just time variation? We think that these small-scale features have wave-like structure. This is due to the use of the 2D FFT. As reviewer 2 pointed out Li et al., (2017) showed that wavelengths in the range of ripples do not necessarily have to be instability features, they can also be secondarily generated small-scale gravity waves. I included this hint and changed the discussion but also abstract and summary accordingly.
P13L29. Better than 'then this means' use 'then this is consistent with' Done
P14L2. Although I agree that causes for ripples at the onset of a SSW are more likely due to changes in static instability, I do not think this conclusion can be inferred from these measurements. Again, it seems to me just a consistency (and not a conclusion) with a smaller dynamical instability. This is in part because your assumption that the large changes in brightness are only due to the generating GW is too strong, but also because of the lack of statistics (just 2 days). Sentence reformulated and message weakened.
Additionally, these conclusions should be put in the context of previous results, which also should be referenced here. Most of the manuscripts concerning ripples only treat single events. The manuscript which is probably based on the largest data set is Li et al. (2017), which I therefore mention it here.
P14L17. Insert 'combined with SABER data' Done
P14L19. 'below the tropospheric jet' --> 'in the troposphere' Done

Fig.2-caption. L5. SABER temperature? VER, thank you
Fig.2-caption: Write SABER channel. Done
Fig.2. Instead of the hard-to-follow description in the caption, just remove non-reliable data according. Number of lines reduced, see answer to comment P8 Sect.4.1. Info now not necessary any more.
Fig. 2. Please, change color code. It is not possible to differentiate most of them from others. Number of lines reduced, see answer to comment P8 Sect.4.1.
Fig. 4, L4. Indicate year of campaign. Done
Fig. 4. For coherence with panel a), include SABER temperatures in panel Done b) and discuss comparisons in text. Done
Fig. 5. The linear fit is not completely convincing. Indicate correlation and discuss in text.
The linear fit can't be convincing since the temperature development, which is not linear either, must also be "visible" in the development of the BV frequency. The linear fit is only to guide the eye. I adapted the figure caption and the description of the figure in section 4.1 ("Between day 1 and 60 of 2016, the OH*-equivalent (angular) BV frequency decreases overall. If one approximates the OH*-equivalent (angular) BV frequency linearly, the approximated values range from ca. 0.022 1/s to 0.020 1/s (Fig. 5, solid line). However, superimposed fluctuations are visible, which reach ca. 13% deviation from the linear fit at maximum.")
Fig. 5-caption: Insert 'SABER' or 'derived from SABER'. Done
Fig. 6. Why do these data end on the 30th and not Feb. 2nd, as in Fig. 4?
In figure 4, nightly mean values are plotted. For the derivation of the GWPED stricter quality criteria apply and the nights in February didn't meet them. Fig 6. L7. GRIPS 9 Done
Figs. 9 and 12. I think that combining these two figures, that is, including the results for the two flights in the same plots would be interesting to see. Done
Fig.14. Lower panel is not needed for the discussion and does not provide additional useful information. Please, remove. But we use this panel, page 14 ll. 29&30 (version with accepted changes).

References

Gerrard et al., Observations of in-situ generated gravity waves during a STE event, Atmos. Chem. Phys., 11, 11913-11917, https://doi.org/10.5194/acp-11-11913-2011, 2011.
Grygalashvyly, M.: Several notes on the OH layer, Ann. Geophys., 33, 923–930, https://doi.org/10.5194/angeo-33-923-2015, 2015.
Garcia-Comas, M., et al.: Mesospheric OH layer altitude at midlatitudes: variability over the Sierra Nevada Observatory in Granada, Spain (37N, 3W), Ann. Geophys., 35, 1151–1164, https://doi.org/10.5194/angeo-35-1151-2017, 2017.

Observations of OH-airglow from ground, aircraft, and satellite: investigation of wave-like structures before a minor stratospheric warming

Sabine Wüst[1*], Carsten Schmidt[1], Patrick Hannawald[2], Michael Bittner[1,2], Martin G. Mlynczak[3], James M. Russell III[4]

[1] Deutsches Fernerkundungsdatenzentrum, Deutsches Zentrum für Luft- und Raumfahrt, , 82234 Oberpfaffenhofen, Germany
[2] Institut für Physik, Universität Augsburg, Augsburg, Germany
[3]NASA Langley Research Center, Hampton, USA
[4]Center for Atmospheric Sciences, Hampton, USA

Correspondence to: Sabine Wüst (sabine.wuest@dlr.de)

Abstract

In January and February 2016, the OH-airglow camera system FAIM (Fast Airglow Imager) measured during six flights on board the research aircraft FALCON in Northern Scandinavia. Flight 1 (14th January 2016) covering the same ground track in several flight legs and flight 5 (28th January 2016) along the shoreline of Norway are discussed in detail in this study. The images of the OH-airglow intensity are analysed with a two-dimensional FFT regarding horizontal periodic structures between 3 km and 26 km horizontal wavelength and their direction of propagation. Two ground-based spectrometers (GRIPS, Ground based Infrared P-branch Spectrometer) provided OH-airglow temperatures. One was placed at ALOMAR, Northern Norway (Arctic Lidar Observatory for Middle Atmosphere Research; 69.28° N, 16.01° E) and the other one at Kiruna, Northern Sweden (67.86° N, 20.24° E). Especially during the last third of January 2016, the weather conditions at Kiruna were good enough for the computation of nightly means of gravity wave potential energy density. Coincident TIMED-SABER (Thermosphere Ionosphere Mesosphere Energetics Dynamics, Sounding of the Atmosphere using Broadband Emission Radiometry) measurements complete the data set. They allow for the derivation of information about the Brunt-Väisälä frequency and about the height of the OH-airglow layer as well as its thickness.

The data are analysed with respect to the temporal and spatial evolution of mesopause gravity wave activity just before a minor stratospheric warming at the end of January 2016. Wave events with periods longer (shorter) than 60 min might mainly be generated in the troposphere (at or above the height of the stratospheric jet). Special emphasis~~ze~~ is ~~put~~ placed on small-scale signatures, i.e. on ripples, which ~~are~~ may be signatures of local instability and which may be related to a step in a wave breaking process. The most mountainous regions are characterized by the highest occurrence rate of wave-like structures in both flights.

1 Introduction

The results presented here are part of the international initiative ROSMIC (Role Of the Sun and the Middle atmosphere/ thermosphere/ionosphere In Climate) and the German program ROMIC (Role Of the Middle atmosphere In Climate). One goal of ROMIC was to investigate coupling mechanisms which connect atmospheric layers from the ground up to the top of the middle atmosphere and vice versa. The project GW-LCYCLE, which was part of ROMIC, addressed questions concerning the life cycle of gravity waves, i.e. their excitation, propagation, and dissipation.

During the field campaign in winter 2015/16 in Northern Scandinavia, ground-based as well as airborne airglow measurements were conducted. At the ground, two spectrometers (GRIPS, Ground based infrared P-branch spectrometer, one at Kiruna, 67.86° N, 20.24° E, and one at ALOMAR, Arctic Lidar Observatory for Middle Atmosphere Research; 69.28° N, 16.01° E) and one camera (FAIM, Fast Airglow Imager, at Kiruna) were operated. An additional FAIM system with small aperture was mounted ~~at~~ on the DLR (Deutsches Zentrum für Luft- und Raumfahrt) research airplane FALCON. Six flights were conducted in January and February 2016 in Northern Scandinavia. The airglow observations refer to the height range of ca. 80–90 km, all other ~~airborne~~ measurements on board the FALCON address heights of ca. 20 km and below. Flight 1 (14th January 2016) covering the same ground track in several flight legs and flight 5 (28th January 2016) with a long flight leg almost parallel to the shoreline of Norway allow for the discussion of different wave activity features and were therefore chosen for a detailed discussion in this study.

Airglow camera measurements on board a research aircraft and therefore covering a wider spatial range are very rare. To our knowledge the only other system with a very good spatial and temporal resolution flown on an aircraft is the one described in Pautet et al. (2016). In contrast to the airglow imaging system (AMTM, Advanced Mesosphere Temperature Mapper) used by ~~Pautet et al. (2016)~~those authors during the DEEPWAVE campaign above New Zealand, the airborne FAIM does not allow for the derivation of OH rotational temperatures. FAIM is based on a InGaAs 320 px × 256 px sensor and integrates over wavelengths from 0.9 µm to 1.65 µm with a temporal resolution of 1 s. ~~The FAIM~~It was optimized for the study of small-scale features (some 100 m to some 10 km depending on the zenith angle and the optics used) in airglow intensity and therefore it has a significantly smaller aperture (in this case 27.3° × 33.9°) and covers a wider spectral range ~~from 0.9 µm to 1.65 µm~~ resulting in a higher spatial and temporal resolution at the sacrifice of geographical coverage (Hannawald et al., 2016). While Pautet et al. (2016) analysed a specific gravity wave event, we concentrate here on the temporal and spatial development of periodic structures in the range of ripples and bands during the two flights mentioned above (section 4.2.2 and 5). Due to this unprecedented spatial and temporal resolution, the focus of this manuscript is especially on the question whether the activity of these small-scale features is enhanced above possible tropospheric gravity wave sources. Furthermore, their activity is studied under different meteorological conditions.

Information about the temporal development of the potential energy density of larger-scale gravity waves are derived based on the GRIPS measurements at Kiruna (section 4.2.1 and 5). Due to varying weather conditions the temporal resolution of

the time series is best during the last third of January 2016. Unfortunately, the weather conditions did not allow these analyses during the same time period for the ALOMAR GRIPS data.

For the calculation of the density of wave potential energy, we compute the (angular) Brunt-Väisälä (BV) frequency based on coincident TIMED-SABER (Thermosphere Ionosphere Mesosphere Energetics Dynamics, Sounding of the Atmosphere using Broadband Emission Radiometry) temperature and OH-B channel volume emission rate (VER) measurements. We use the latter also in order to learn more about the OH-layer height and thickness (section 4.1 and 5).

All results are interpreted in the context of the minor sudden stratospheric warming (SSW) which happened at the end of January 2016 (Dörnbrack et al., 2018). As SSW events are associated with dynamical changes in the stratosphere and mesosphere over several days, effects on gravity waves in the upper mesosphere / lower thermosphere can be expected and have also already been observed and/or modelled: Yigit and Medvedev (2012), for example, report that GW activity increases by a factor of 3 in the course of the warming modelled by them. Liu (2017) point out that at high latitude in the winter hemisphere the momentum flux varies rapidly during the SSW. Afterwards, the magnitude of the mesospheric momentum flux decreases significantly. His findings agree with the observations of GW momentum flux changes during a SSW published by Wright et al. (2010), France et al. (2012), Thurairajah et al. (2014) and Ern et al. (2016), for example. Liu (2017) argues that the rather rapid change of the winter jet system is expected to be a source of GW variability during SSW as GWs can be excited by imbalance of jet flow (O'Sullivan and Dunkerton 1995; Zhang 2004).

Formatiert: Schriftart: Nicht Fett, Schriftartfarbe: Automatisch

2 Data

2.1 GRIPS

During winter 2015/16, ground-based airglow observations were carried out with the infrared spectrometers GRIPS 9 at Kiruna (67.86° N, 20.24° E), Sweden and GRIPS 14 at ALOMAR (Arctic Lidar Observatory for Middle Atmosphere Research; 69.28° N, 16.01° E), Norway.

GRIPS instruments are based on a monochromator with 163 mm focal length (Czerny-Turner setup with crossed beam configuration) and a thermoelectrically cooled 512 px InGaAs photodiode array. They observe ~~the OH(3-1) and the OH(4-2) vibrational transitions in~~ the spectral range between 1.5 µm and 1.6 µm, which includes OH(3-1) and OH(4-2) vibrational transitions (OH(3-1) Q- and P-branches, OH(4-2) R- and Q-branches up to the first line of the OH(4-2) P-branch). The spectral resolution is ca. 3.1 nm at a wavelength of 1550 nm~~In standard setup, the temporal resolution is 15 s (Schmidt et al. 2013)~~. The field of view (FoV), over which the instruments integrate, is mainly governed by the F-number of the polychromator (#F3.6) because the instrument is operated with no further objective lenses. In standard setup, the temporal resolution is 15 s. Details about the instrument are provided in Schmidt et al. (2013).

Rotational temperatures are derived operationally from the first three P_4 lines of the OH(3-1) ~~P branch~~ transition, $P_1(2)$, $P_1(3)$, and $P_1(4)$. Under the assumption of local thermodynamic equilibrium, the intensity of these lines follows a Boltzmann distribution. The only variable on which this distribution depends is the temperature. Therefore, the relation of the intensity of these lines allows calculating the rotational temperature, Einstein coefficients and term values of the respective rotational level provided (Meinel, 1950, Krassovsky et al., 1962, Mies, 1974, Schmidt et al., 2013).

In this study, one minute mean and nightly mean temperature are used. ~~They~~ One minute mean values typically ~~exhibit uncertainties~~have a precision of up to ±8 K ~~at this temporal resolution~~(from error propagation calculation of the 15s values), but the exact value strongly depends on the emission intensity, which can be highly variable. Due to the high number of measurements, the error of nightly mean values is much lower. For the temperature derivation, the measured spectrum between 1.5 µm and 1.6 µm is approximated using a low pass filter. The uncertainty is calculated from the standard deviation of the residuals. It is influenced by the observations conditions and by the instrument itself (readout noise of the detector, which is assumed to be constant, the photon or shot noise and the dark current noise, which both refer to statistical variations and scale with the square root of the signal level and dark current level). The average pattern of the dark current noise along the photodiode array as well as a constant noise value are retrieved and subtracted. The major sources of uncertainty are therefore bad weather conditions (background intensity is increased by modulated by H_2O absorption in the lower atmosphere), which disturb the noise reduction or make it impossible. Details about the temperature retrieval and the noise reduction are also provided in Schmidt et al. (2013). Airglow observations are only performed during darkness ~~and d~~. Dense cloud coverage poses an obstacle for the measurements, thin clouds or fog increase the error.

At Kiruna, GRIPS 914 observed the airglow layer at a fixed zenith angle of 0°. Its ~~field of view (~~FoV~~)~~ was approximately 25 km x 25 km. GRIPS ~~9~~14 at ALOMAR was operated in a scanning mode (the FoV is changed four times within one

Formatiert: Tiefgestellt

Formatiert: Nicht Hervorheben

Formatiert: Tiefgestellt

minute then starting with the first ~~one~~ FoV again, azimuth and zenith angles: (120°, 30°), (0°, 30°), (240°, 30°), (not available, 0°)) with one FoV in zenith direction. Concerning the size of the FoV, the time series referring to zenith direction at ALOMAR is comparable to the measurements at Kiruna. For more information about the GRIPS system, operated in standard and in scanning mode, see Schmidt et al. (2013), Wachter et al. (2015), and Wüst et al. (2018).

Observations at ALOMAR were performed between December 5, 2015 and February 3, 2016. Observations at Kiruna were carried out between January 14 and February 2, 2016. During the latter time period, the weather at ALOMAR was very variable. Information about gravity wave potential energy density (GWPED) according to Wüst et al. (2016) and the data quality criteria given therein were therefore not derived for ALOMAR. Nightly-mean temperatures, however, were successfully retrieved for 56 out of 61 nights at ALOMAR and for 19 out of 19 nights at Kiruna.

2.2 FAIM

Two-dimensional airglow observations were performed by FAIM (Fast Airglow Imager, for details about the ground-based instrument see Hannawald et al., 2016) on board ~~of~~ the DLR aircraft FALCON.

The spectral range, over which the ~~-~~instrument integrates every second, is 0.9 µm–1.65 µm, ~~the integration time is 1 s,~~ the ~~sensor~~ size of the InGaAs sensor is 320 px ~~×~~× 256 px (model "Xeva" manufactured by Xenics nv). The intensities recorded by FAIM include different airglow emissions (oxygen and hydroxyl), however, the influence of OH airglow dominates. The instrument is equipped with a three-stage thermoelectric cooler. Due to limited available space, the instrument was mounted ~~at~~ on the headmost aperture plate position of the aircraft. The observations were performed in near zenith direction (roll angle of the instrument w.r.t. the aircraft plane: -5°). The aperture angle of the optics was mainly limited by the small diameter window (approx. 70 mm), so a lens system with opening angles of 27.3° ~~×~~× 33.9° was used (larger angles resulted in stronger vignetting). In order to maximise the geographical coverage, the camera was mounted with a yaw angle of -45°, making the image diagonally oriented to the flight track (compare Fig. 7 and 10). The spatial resolution was approximately 167 meters per pixel, the FoV covered an area of 43 km ~~×~~× 55 km. The exact values depend on ~~the~~ roll (25° at maximum), ~~yaw~~ and pitch (0°–5°) angles as well as on the height of the aircraft. The high temporal and spatial resolution allows especially the investigation of gravity waves with short wavelengths and short periods along the flight track.

During the GW-LCYCLE campaign, six night-time flights were conducted above Northern Scandinavia. At least large parts of the flights took place above the tropospheric cloud level. The camera delivered data for all six flights. Flight 1 (14th January 2016) and flight 5 (28th January 2016) were least disturbed by aurora or moon light. Therefore, they are subject of this study.

Additionally, an all-sky FAIM system was operated at Kiruna from January, 14th 2016 to February, 2nd 2016. Due to low level clouds or fog at the times of the aircraft overpasses as well as some water vapour condensation occurring on the entrance optics during the very cold nights (-40°C), only few nights of this ground-based imager can be analysed. Therefore, these measurements are not ~~subject of further analysis~~part of ~~here~~ this publication.

Formatiert: Schriftartfarbe: Automatisch, Englisch (USA), Nicht Hervorheben

Formatiert: Schriftartfarbe: Automatisch, Nicht Hervorheben

Formatiert: Schriftartfarbe: Automatisch, Nicht Hervorheben

2.3 TIMED-SABER

The TIMED satellite was launched on 7 December 2001 and the on-board limb-sounder SABER delivers vertical profiles of kinetic temperature on a routine base from approximately 10 km to more than 110 km altitude with a vertical resolution of about 2 km until today (vertical sampling 300–400 m). The high vertical resolution is suitable for the investigation of gravity wave activity. About 1200 temperature profiles are available per day. The latitudinal coverage on a given day extends from about 53° latitude in one hemisphere to 83° in the other. Due to 180° yaw manoeuvres of the TIMED satellite this viewing geometry alternates once every 60 days (Mertens et al., 2004; Mlynczak, 1997; Russell et al, 1999). ~~A variety of SABER publications is available, and an overview is given on http://saber.gats-inc.com/publications.php.~~

Kinetic temperatures are derived from the 15 µm CO_2 emissions. One of the main problems of deducing kinetic temperature values in the mesosphere and upper ~~levels~~ heights ~~is~~ are ~~certainly~~ non-LTE conditions (NLTE), i.e. conditions that depart from Local Thermodynamic Equilibrium. NLTE algorithms for kinetic temperature were employed in the SABER temperature retrieval in version (v) 1.03 (Lopez-Puertas et al., 2004) as well as in ~~versions,~~v-1.04 and 1.06 (Mertens et al., 2004, 2008). In ~~version~~ v1.07, further improvements were made: CO_2 profiles from the Whole Atmosphere Community Climate Model (WACCM) ~~are~~ were used in the retrieval algorithm in order to remove inconsistencies in the vertical structure of diurnal temperature tides (Remsberg et al., 2008), for example. A discussion of SABER v1.07 is provided by Remsberg et al. (2008) and García-Comas et al. (2008). The WACCM results integrated in v1.07 were scaled to match a CO_2 trend model. V2.0 now uses CO_2 from an updated WACCM model. Furthermore, some reaction rates were changed in the CO_2 vibrational temperature model. Finally, this newest data version relies on recalibrated SABER radiances and on retrieved [O] values for all data (v1.07 used retrieved [O] for daytime measurements only and where the solar zenith angle < 85°). The information concerning v2.0 is taken from Dawkins et al. (2018).

~~Comparisons with reference data sets generally confirm the good quality of SABER temperatures. In the stratosphere and lower mesosphere biases of 1 K to 3 K are indicated (SABER temperatures are too high by 2–3 K in the lower stratosphere, too low by 1 K in the upper stratosphere and by 2–3 K in the mid-mesosphere). Due to noise effects, increased uncertainties have to be expected in the UMLT region. Comparisons to LIDAR and airglow measurements show differences of 10 K and more (Remsberg et al., 2008).~~ Those authors also compared SABER temperature data v2.0 between 75 and 105 km with data from nine ground-based lidars deployed at different latitudes (Spitsbergen at 78.0°N, ALOMAR at 69.3°N, Kühlungsborn at 54.1°N, Boulder at 40.1°N, Fort Collins at 40.6°N, Logan at 41.7°N, Arecibo at 18.4°N, Cerro Pachon at 30.3°S, and McMurdo at 77.8°S). Also for this SABER version holds that the kinetic temperatures (more precisely the seasonal mean in this case) derived by the satellite and the validation instrument agree well. The smallest absolute temperature difference is found between 85 and 95 km height, where the respective SABER and lidar uncertainties were smallest.

Formatiert: Tiefgestellt
Formatiert: Tiefgestellt
Formatiert: Tiefgestellt
Formatiert: Englisch (USA)
Formatiert: Englisch (USA)
Formatiert: Englisch (USA)
Formatiert

We use TIMED-SABER temperature and OH-B channel data (volume emission rates, VER) in its latest version (2.0) within a square of 300 km edge length centred at ALOMAR and between 17 and 5 UTC for the derivation of additional information about the OH-airglow layer characteristics and about the (angular) Brunt-Väisälä (BV) frequency at mesopause height. These values are also taken for Kiruna, since both locations are not more than 300 km away from each other. For heights of 80–90 km, precision, systematic errors, and accuracy are specified with 1.8–3.6 K, 1.4–4.0 K, and 2.3–5.4 K for a single profile (according to Dawkins et al. (2018) who reproduced these figures from saber.gats-inc.com).

Formatiert

The OH-B channel covers the wavelength range from 1.56 to 1.72 µm, which includes mostly the OH(4-2) and OH(5-3) vibrational transition bands. The mean height difference between the OH(4-2)- and the OH(3-1)-emission, which is addressed by the OH*-spectrometers mentioned above, is approximately 500 m (von Savigny et al., 2012). Therefore, ~~and therefore negligible compared to the FWHM~~aspects derived from the OH-B channel concerning vertical movements, for example, also hold for the OH(3-1) layer.

The data was downloaded from the SABER homepage (saber.gats-inc.com).

3 Analysis

3.1 Derivation of wave potential energy density

From the GRIPS data, we derive the density of gravity wave potential energy E_{pot} (GWPED) according to

$$E_{pot} = \frac{1}{2}\frac{g^2\overline{\hat{T}'^2}}{N^2} \quad (1)$$

where

g is the acceleration of gravity, (g=9.6 m/s² taking into account its height-dependence),

N the (angular) BV frequency, and

$\hat{T}' = T'/\hat{T}$ the normalized temperature fluctuation. The overbar denotes the nightly average.

E_{pot} is calculated for different period ranges. It is distinguished between periods ~~(~~shorter and longer than 60 min as they show different overall evolvement (concerning annual and semi-annual oscillations, for example)~~)~~. The extraction of the temperature fluctuations is based on the iterative calculation of sliding means. Since this approach results in a shortening of the smoothed data series, data of gaps of 20 min at most are interpolated and the time series is mirrored at the beginning and the end. Details can be ~~looked~~ found~~up~~ in Wüst et al. (2016).

For the derivation of the (angular) BV frequency N vertically-resolved temperature profiles are needed:

$$N = \sqrt{\frac{g}{T}\left(\frac{dT}{dz} + \Gamma\right)} \quad (2)$$

where

z is the height,

T is the temperature and

Γ the dry adiabatic lapse rate with 9.6 K/km.

Since GRIPS provides a temperature value which is vertically averaged over the OH*-layer, additional data are necessary for the calculation of N. As in Wüst et al. (2016, 2017a, 2017b), TIMED-SABER temperature information ~~are~~ is used for this purpose. The OH*-equivalent (angular) BV frequency is calculated for the day of year (DoY) 1–60 of 2016 by weighting the height-dependent squared BV-frequency values with the volume emission rate (VER) profiles. From time to time, the maximum of the VER is observed around 40 km in SABER profiles. Therefore, the calculation is restricted to the height range between 71 and 97 km (84 km ± 13 km, the height of 84 km corresponds to the mean ~~OH* layer~~ height of maximum VER derived by Wüst et al. ~~,~~ (2016) around ALOMAR based on SABER OH-B channel measurements for one year, in general slightly higher values are reported for other stations or other time periods, see Wüst et al. (2016, 2017a, 2017b) or Baker and Stair (1988)). Since the SABER profile provides only a snapshot of the atmospheric situation, an error of 10% is assumed. This value ~~catches~~ includes the day-to-day variability (Wüst et al., 2017b).

Formatiert: Nicht Hervorheben

Formatiert: Nicht Hervorheben

3.2 Spectral analysis

In order to analyse the FAIM measurements, a two-dimensional Fast Fourier Transform (2D FFT) is applied. Sequences with high roll and pitch angles as they occur during turning manoeuvres were excluded since the size of the FoV and the spatial resolution change significantly within a short time. A steady shaking of the airplane limits the application of the 2D FFT: ~~phase information of consecutive images cannot be used to derive additional parameters such as period and phase speed.~~The shaking translates the FoV by several pixels in a quasi-periodic manner and applies a motion blur on the images. The translation does not allow deriving the change of the phase from consecutive images, but this information is crucial for calculating phase speed and period of the waves. The translation affects the whole image and therefore all wave crests within the image, the wavelength, which is derived for each image individually, is not influenced. The motion blur does not change the position of the wave crests, but it reduces the amplitude of the waves. The amplitude, however, is not used here. O~~o~~nly horizontal wavelength and the direction of propagation with a 180° ambiguity are computed.

The ~~used~~ 2D FFT algorithm employed needs equidistant data. Therefore, the images are un-warped. As mentioned above, the camera is deployed at a roll angle w.r.t. the plane of -5° and at a yaw angle w.r.t. the plane of -45°. Therefore, two rotation matrices (one for the yaw axis and one for the roll axis) are used to convert the reference system of the instrument to the reference system of the airplane. The orientation of the airplane is also characterized by a roll, pitch, and yaw angle. Therefore, three rotation matrices are then applied to transform the reference system of the airplane to a world coordinate system (azimuth and elevation relative to the Earth's surface). The three required angles are taken from the flight metadata which are given with a temporal resolution of 1 s. The new pixel positions are then calculated by projecting the image in world coordinates to the airglow layer at 87 km height. Changes in the airglow layer altitude have only minor effects on the results (+/-5 km in the altitude layer corresponds to +/- 6% in the resolution and therefore also in the horizontal wavelength, calculated for a zenith angle of 5°). An additional flipping at the North-South axis brings the image to a satellite's view perspective. The scale is kept constant with 167 m/px (or 6 px/km) for all images allowing direct comparison of images at different times and angles. Before analysing the un-warped images, the stars in the images need to be removed since otherwise their signal may influence the 2D FFT spectra. This is done by applying a sliding median blur with a kernel of 17 ×~~x~~ 17 px.

All images are ~~cropped~~ reduced to 26 km ~~x~~× 26 km. This is the largest square size which does not contain any pixels outside the un-warped image region (marked in Fig. 1).

For each image, the mean is subtracted and a Kaiser-Bessel window (α=4) is applied to let the borders of the area steadily decrease to zero. Zero-padding further optimises the calculation of the 2D-FFT.

After calculating the 2D FFT for each image (each flight consists of ca. 12,000 images), wavelength and angle of propagation are extracted for every significant peak in the spectrum (Monte-Carlo significance test with a significance level of 95%).

Formatiert: Schriftartfarbe: Automatisch

The algorithm is described in detail in Hannawald et al. (201~~8~~9).

Formatiert: Block, Zeilenabstand: 1,5 Zeilen

4 Results

4.1 Height, thickness and intensity of the OH-layer

During winter (DoY 1–60) 2002–2016, the averaged maximum of the volume emission rate, in the following denoted as OH*-layer height, and its averaged full-width a half maximum (FWHM) around ALOMAR vary between ca. 840.50–868.0 km and 76.0–710.5 km, respectively, based on SABER data (see Fig. 2 (a) and (b) for a comparison with the mean over all ~~other~~ years, and Fig. 3 (a) and (b) for details about the year 2016). Compared to the mean over all ~~other~~ years, the FHWM for 2016 (thick blue line) can be characterized as low especially during the end of January and large parts of February. It shows a drop centred at DoY 43. The OH*-layer height is stable at 85.0–85.5 km until DoY 23 and ~~starts to~~ rises by 2.5 km during the following ten days. Afterwards, it ~~varies~~ oscillates around ca. 87.5 km. Compared to the mean over all ~~other~~ years, the OH-airglow layer altitude increases and its width decreases from DoY 23 on.

Both, ground-based GRIPS and space borne SABER observations of the OH intensity, agree fairly well during the GW-LCYCLE campaign (see Fig. 4a). In the case of SABER, the peak intensity is used, which correlates very well with the intensity integrated over the analysed height range (R^2 of about 87%). The GRIPS instruments deliver only relative intensities. They are normalized to their respective mean. In particular, the intensities~~y~~ of GRIPS and SABER show ~~a~~ pronounced periodicities~~y~~ in the range of some days~~of ca. 4–6 days~~. At the end of January and the beginning of February, the intensities of all instruments~~y~~ reach~~es its~~ their absolute minimum.

The same characteristics hold also for the temperature derived by the GRIPS instruments ~~at ALOMAR and Kiruna~~ and the VER-weighted temperature calculated from SABER (see Fig. 4b). Over all, temperature and intensity show similar relative variations. The absolute temperature difference between GRIPS and SABER measurements referring to ALOMAR varies between ca. 0 K and 18 K. This difference is not unusual for this height range, altitude and season when taking into account that the SABER and GRIPS measurements do not match exactly in place, time and addressed air volume (Wendt et al., 2013).

4.2 Periodic signatures

4.2.1 Horizontal wavelengths longer than ca. 25 km

Due to the FoV of GRIPS 9 at Kiruna, the instrument is sensitive to horizontal wavelengths of 25 km and longer. As mentioned in section 3.1, the OH*-equivalent (angular) BV frequency is calculated based on SABER temperature measurements in order to compute GWPED from GRIPS. Between day 1 and 60 of 2016, the OH*-equivalent (angular) BV frequency decreases overall. If one approximates the OH*-equivalent (angular) BV frequency linearly, the approximated values ~~nearly linearly from approximately~~range from ca. 0.02~~3~~2 1/s to 0.02~~1~~0 1/s (Fig. 5, ~~dashed~~ solid line). However, ~~showing~~ superimposed fluctuations are visible, which reach ca. 13% deviation from the linear fit at maximum.

According to the data quality criteria for the GWPED calculation from GRIPS data (availability of at least 4 h of good quality data and exclusion of artefacts due to sunset and sunrise) as mentioned in Wüst et al. (2016), information about the energy content of gravity waves ~~are~~ is derived between the nights from 13th to 14th and 30th to 31st January, 2016 based on GRIPS 9 measurements at Kiruna (a~~.~~s already mentioned above, the weather situation at ALOMAR did not allow the derivation of gravity wave information there).

For periods longer (shorter) than 60 min, the energy density varies between 10 and 160 J/kg (5 and 17 J/kg) with a mean of 43 J/kg (9 J/kg) (Fig. 6). Relative to these means, individual values lie within an interval of -77% and + 192% (-38% and +45%) for long (short) periods. The potential energy density of gravity waves with periods longer than 60 min can therefore be characterized as being more variable compared to periods shorter than 60 min. Fitting a cubic spline (non-iterative version as described in Wüst et al., 2017c) to the GWPED values suggests that a minimum of GWPED is observed around January 21st and 22nd and a maximum around January 27th for periods longer than 60 min. This overall behaviour cannot be confirmed for periods shorter than 60 min.

4.2.2 Horizontal wavelengths shorter than ca. 25 km

Wavelengths shorter than 25 km can be analysed using data of the airborne FAIM. The route of the first flight forms a triangle with the last two flight legs roughly parallel to a circle of longitude and latitude. The diagonal connection between Kiruna and approximately ALOMAR was covered three times in a row (Fig. 7). Although this flight track allows in princip~~a~~le the investigation of horizontal structures much larger than the FAIM FoV (via comparison of the individual flight legs), the airglow brightness varied too fast during the entire flight for achieving unambiguous results. This is especially apparent in the diagonal flight legs (Fig. 8a). Therefore, we concentrate on the analysis of horizontal structures in the range of the FoV size. As mentioned in section 2.2, the FoV is ca. 43 km x 55 km at 90 km height. However, its size changes with varying roll and pitch angles.

Figure 7 shows time difference images (time difference: 10 s) of the first flight. A difference image is derived by subtracting the intensity measured by each pixel from the intensity measured 10 s later by the same pixel. The velocity of the airplane is approximately 210 m/s. So, the airplane moves ca. 2 km in 10 s. Calculating a difference image emphasizes horizontal structures which change significantly within 2 km and/or within 10 s in flight direction. In the case of gravity waves, the result depends on the horizontal wavelengths and on the horizontal phase speed. For gravity waves with zero phase speed, constructive interference appears for a horizontal wavelength of 4 km in flight direction. The longer the wavelength, the less

it will be emphasized. Destructive interference happens for horizontal wavelengths of 2 km (divided by integer factors) in flight direction. However, the above-mentioned constant shaking of the aircraft aids that also these small structures can at least to some extent be identified in the images. So, one can say calculating a difference image is equivalent to applying some (high-pass) spectral filtering and amplification algorithm. The difference images of the first flight show wave-like structures of different wavelengths and amplitudes. There exists almost no region where such structures cannot be observed.

In order to derive quantitative results, the original (non-difference) images are analysed with a 2D FFT. Details about the different analysis steps are given in section 3.2. The shortest wavelength to which the FFT i~~n~~s sensitive is ca. 3 km (due to pre-processing with median blur applied to 17 pixels, 6 pixels correspond to 1 km). The FoV is ~~cut~~ reduced to 26 km ~~×~~ 26 km.

It becomes clear that wave numbers and intensities vary in time and space (see Fig. 8b). In flight 1, high Fourier amplitudes also in the range of small-scale features (wavelength of 15 km wavelength and less) appear approximately between 16:20 UTC and 16:35 UTC (flight leg 1, turning manoeuver needs to be excluded) and between 17:30 and 18:00 UTC (flight leg 2 and 3). Between 18:30 UTC and 18:55 UTC (flight leg 4 and 5) especially small-scale features are relatively pronounced while larger-scale features are weaker compared to the time periods just mentioned. During these three time periods, the airplane was located east and/or southeast as well as above the Scandinavian mountain chain. The airglow brightness averaged over each picture shows local maxima during these three time periods (Fig. 8a).

Summarized over the whole flight, structures with wavelengths longer than 15 km propagate more frequently to the southeast (and/or northwest) than to the northeast (and/or southwest, Fig. 9). The majority of wavelengths shorter than 15 km moves to the northeast (and/or southwest). We identified 73 (31) events with wavelengths longer (shorter) than 15 km.

During the fifth flight on January 28th, 2016, airglow observations were performed on the return from Karlsbad, Southern Sweden, over Bergen, Southern Norway, along the coast line of Norway back to Kiruna (Fig. 10). The flight route can be divided into three legs. Several oscillations with 20–25 km are clearly visible at the beginning and at the end of the flight track. Especially, during the second (latitude-parallel) leg, many superimposed small structures with different orientations can be seen. The airglow intensity averaged over each image shows wave-like structures during each flight leg (Fig. 11a). They are most pronounced in flight leg 3. ~~The horizontal wavelengths (in flight direction) reach 75–100 km (from Fig. 11a under the assumption that the phase speed of the wave is negligible w.r.t. the speed of the plane with ca. 210 m/s).~~

Regions characterized by pronounced wave activity are observed especially after 18:30 UTC (Fig. 11b, mostly flight leg 3). During this time, the airplane flew along the coast line of Norway or above the Scandes. In contrast to flight 1, airglow brightness (averaged over each image) is maximal before the time period of maximal (Fourier) intensity.

Flight 5 also differs from flight 1 concerning the propagation directions (Fig. 12): wavelengths longer than 15 km propagate mostly to the northeast (and/or southwest), for wavelengths shorter than 15 km a preferred quadrant of propagation cannot be

identified. A pronounced maximum can be found for eastward (and/or westward) propagation direction. In this direction nearly no larger-scale waves move. We identified 113 (63) events with wavelengths longer (shorter) than 15 km.

The occurrence rate of wave events varies during one flight and from flight to flight (Fig. 13). Overall, the legs of flight 5 show less variability than the legs of flight 1.

For both flights, the zonal legs (leg 5 of flight 1 and leg 2 of flight 5), where the airplane flew most of the time over the mountain chain and passed the highest elevations of the respective flight routes (grey line in Fig. 8a and 11a), are characterized by the highest occurrence rate (ca. factor 1.8–4.5 enhanced compared to the leg with the lowest occurrence rate of the respective flight). This agrees quite well with the visual inspection of the difference images of flight 5 (Fig. 10). For flight 1, this result is due to a large portion of small-scale wave-like structures (3–15 km wavelength) in leg 5.

The diagonal legs 1, 2 and 3 of flight 1 are identical concerning the route, however, the occurrence rate varies: it is highest in leg 2 and lowest in leg 3 (factor of ca. 2.6).

5 Discussion

Stratospheric winds varied strongly during ~~the~~ January 2016 (Fig. 14). This was due to a minor stratospheric warming at the end of January (Dörnbrack et al., 2018). It was one of three consecutive minor stratospheric warmings which occurred before the final breakdown of the polar vortex at the beginning of March 2016 (Manney and Lawrence, 2016). Starting mid-January 2016, ~~T~~the polar vortex became disturbed by planetary waves; especially planetary waves of zonal wave number 1 were amplified in the second half of January (Manney and Lawrence, 2016). Consequently, the vortex was displaced southward with its centre between Svalbard and Northern Scandinavia and the polar night jet became elongated in west-east direction (strong curvature over the Northern Atlantic and over Siberia, Dörnbrack et al., 2018). From January, 26th to February, 1st 2016, the meteorological regime above Kiruna was characterized by the transition of the stratospheric flow during the minor warming. After 30 January 2016, the horizontal wind in the stratosphere was rather light (< 20 m/s) and the stratopause was relatively warm (290 K, Dörnbrack et al., 2018). A stratospheric warming should affect the residual circulation and therefore the OH-layer characteristics. When stratospheric winds weaken or even reverse, filtering of gravity waves generated further down is changed. When there is a stratospheric wind weakening or reversal, the downward movement in the mesopause, which is part of the residual circulation, weakens and this influences the OH excitation mechanism. However, planetary wave activity complicates this simplified picture: transmission of gravity waves is then a function of longitude (Whiteway and Carswell (1994), Dunkerton and Butchart (1984), and references in both publications).

~~Neglecting the effect of planetary waves, w~~We expect the following effect on the zonal means. The OH excitation mechanism is dominated by atomic oxygen which is produced at higher altitudes in the atmosphere (Shepherd et al., 2006). Processes which lead to vertical transport of atomic oxygen influence the OH volume emission rate, but also height and thickness of the OH*-layer (see also, Liu and Shepherd, 2006; Mulligan et al., 2009; Grygalashvyly, 2015; von Savigny, 2015; Garcia-Comas et al., 2017). On average, height and thickness as well as height and intensity are anti-correlated. So, a weakening of the residual circulation should lead to a higher OH-airglow altitude, to a thinner OH-airglow layer, to a reduced OH-airglow intensity, and to a lower temperature. According to SABER measurements ~~T~~the temporal development of the airglow-layer characteristics observed at the end of January ~~2016~~ and during February 2016 is consistent with the described expectations before and during a stratospheric warming.

Additional to the OH-layer characteristics, we also analysed periodic structures of different horizontal wavelengths. In literature, wave-like horizontal structures are often divided into ripples and bands. Ripple structures are phenomena with horizontal wavelengths of 5–15 km (Li et al., 2005, Taylor et al., 1995) or of 20 km at most (Takahashi et al., 1985). Their lifetime is in the range of 45 min and less (Hecht, 2004). Fronts with large horizontal extent and wavelength, which can be sometimes observed for hours, are usually called bands (Taylor et al., 1995; Clairemidi et al., 1985). Hecht (2004) summarizes in his table 1 band and ripple characteristics based on four literature studies: the observed periods of ripples

Formatiert: Hochgestellt

Formatiert: Hochgestellt

Formatiert: Nicht Erweitert durch / Verdichtet durch

Formatiert: Nicht Erweitert durch / Verdichtet durch

Formatiert: Zeichenskalierung 100 %, Nicht Erweitert durch / Verdichtet durch

(close to 5 min) are shorter than the ones for the bands, this also holds for the horizontal wavelengths. However, the provision of exact values does not seem to be possible.

In most studies, ~~R~~ripples are interpreted as signatures of local instability and may be related to or also be part of a breaking process of an atmospheric gravity wave (e.g., Li et al., 2005; Hecht, 2004; Fritts et al., 1997). In this case, ~~T~~they move with the background wind and can be separated into convective and dynamical ones according to their generation process (convective and dynamical instability, which occur for a Richardson number of less than 0 and 0–0.25, respectively). Ideally, the phase fronts of the dynamical (convective) ripples are oriented parallel (perpendicularly) to the associated gravity wave. However, also other cases have been observed (Hecht, 2004). Li et al. (2017) showed that more than half of the ripples they observed with an OH all-sky imager at Yucca Ridge Field Station, Colorado (40.7°N, 104.9°W), from September 2003 to December 2005 do not advect with the background winds and might not be instability features but wave structures that are hard to be distinguished from real instability features. In this case, the ripples could be related to the secondarily generated small-scale gravity waves (Vadas et al., 2003; Zhou et al., 2002).

Formatiert: Nicht Hervorheben

Formatiert: Nicht Hervorheben

In our airborne measurements, we find horizontal wavelengths in the range of ripples and bands. ~~-~~ Concerning the latter we can argue that ~~T~~the chance to measure low-frequency (inertia) waves by FAIM is very much reduced compared to waves with higher frequencies. This can be deduced as follows. The higher the intrinsic frequency of a wave is, the smaller the angle between the ~~steeper the~~ wave fronts ~~(with respect to~~and the vertical must be~~) are~~. The horizontal wavelengths derived from the FAIM data are 26 km at maximum. Since the OH* layer extends over some kilometres, vertical wavelengths in the range of the full width at half maximum can barely be detected (Wüst et al., 2016). However, ~~T~~the vertical wavelengths of low-frequency waves are much smaller than the horizontal ones. Therefore, we can argue that FAIM is not very sensitive to low-frequency waves. GRIPS is less sensitive to short horizontal wavelengths than FAIM. In this study, the FoV of GRIPS is approximately 25 km x 25 km. Therefore, the signal of horizontal wavelengths in the range of 25 km and less is very much reduced or entirely averaged out. The argumentation concerning the resolvable vertical wavelength is the same as for FAIM. Therefore, GRIPS is less sensitive to high-frequency waves than FAIM.

~~. Since the OH* layer extends over some kilometres, vertical wavelengths in the range of the full width at half maximum can barely be detected (Wüst et al., 2016).~~

Conclusions about possible sources of the observed bands are very difficult without a ray tracer since wind and temperature change with height influencing the angle of the wave front to the vertical.

However, we can conclude the following.

Especially mountain waves (phase velocity equal to zero) generated near Kiruna had best chance to reach the OH-airglow layer around January 21st and from January 24th to 28th. During the other time periods, the horizontal wind speed became

zero in extended height intervals (Fig. 14), which prohibits a vertical propagation (Fritts and Alexander, 2003). Indeed, we observed the highest occurrence rate of band-like structures in FAIM measurements during flight 5 (January 28th) when the airplane flew most of the time over the mountain chain and passed the highest elevations of the flight route.

The propagation of gravity waves with non-zero wind speed is discussed now. Before January 25th, zonal winds in the upper stratospher~~ic~~e ~~jet was~~were ~~faster~~ stronger than in the upper troposphere ~~one~~ above Kiruna (Fig. 14). Zonal winds in the stratosphere became weaker after Jan 23rd. ~~D~~During January 25th and 28th, ~~the~~ zonal winds in the troposphere and in the stratosphere ~~was~~ were of comparable (eastward) velocity. So, for gravity waves generated in the troposphere, the stratospheric jet was not an additional filter and more waves should reach the OH airglow layer. ~~.~~After January 28th, the vertical profile of the zonal wind showed regions of positive and negative wind velocity. An enhanced gravity wave filtering (for waves which had to pass the different regions) could therefore be expected. This agrees with the temporal development of the density of wave potential energy (periods longer than 60 min) derived from GRIPS, which depicts a maximum around the 27th of January (Fig. 6). It also agrees with the number of wave events observed by the airborne FAIM, which increased by a factor of 1.5–2.0 from flight 1 on January 14th to flight 5 on January 28th (the observation time of wave events, i.e. the time between the observation of the first and the last we event, changed only from 2.5 h to 2.9 h from flight 1 to flight 5). For gravity waves with periods shorter than 60 min, the temporal development of the GWPED derived from GRIPS measurements shows less and different variations. A significant maximum around January 26th might be present, at least compared to January 18th/19th and 28th.

A similar increase, in these cases of gravity wave activity or momentum flux, during a SSW is also reported by other authors. Yiğit and Medvedev (2012), for example, used a global circulation model in order to show that the activity of GW of lower atmospheric origin is enhanced by a factor of 3 in the course of the modelled warming. Based on WACCM (Whole Atmosphere Community Climate Model) Liu (2017) point out that the magnitude of the mesospheric momentum flux decreases significantly after the SSW event, but it varies strongly during the event. His findings agree with the observations of GW momentum flux changes during a SSW published by Wright et al. (2010), France et al. (2012), Thurairajah et al. (2014) and Ern et al. (2016), for example. An overview about the recent progress in understanding the role of gravity waves in vertical coupling during SSW is given by Yiğit and Medvedev (2016).

It is possible that the GW enhancement in the mesosphere is not only due to less filtering of tropospheric GW, the GW source could also be at higher altitudes. Liu (2017) argues that the rather rapid change of the winter jet system is expected to be a source of GW variability during SSW as GWs can be excited by imbalance of jet flow (O'Sullivan and Dunkerton, 1995; Zhang, 2004). Gerrard et al. (2011) find evidence that upward propagating gravity waves were generated in situ by a stratospheric temperature enhancement. However, as described above, the stratopause was relatively warm after January 30th (290 K, Dörnbrack et al., 2018) when our measurement period came to an end. The maximum in GWPED was observed earlier.

Compared to the zonal wind, the meridional component evolves differently (Fig. 14c): the direction of the meridional wind varies over the whole height range between January 20th and 27th, 2019. Afterwards, this is not the case any more. If gravity

Formatiert: Hochgestellt
Formatiert: Hochgestellt
Formatiert: Hochgestellt
Formatiert: Hochgestellt
Formatiert: Hochgestellt
Formatiert: Hochgestellt
Formatiert: Hochgestellt
Formatiert: Hochgestellt
Formatiert: Hochgestellt

wave filtering was driven by the meridional wind, one would expect that the activity of gravity waves generated in the troposphere increases at the end of January. This is not the case for our GRIPS observations.

Therefore, according to GRIPS data we conclude that the SSW affects gravity waves with periods longer and shorter than 60 min differently. The GWPED development for~~gravity waves with~~ periods longer than 60 min is consistent with the assumption of a tropospheric source. However, we can also not exclude that at least parts of observed gravity waves are generated at higher altitudes. The GWPED development for periods shorter than 60 min is less consistent with the assumption of a tropospheric source.~~could to a larger part be generated in the troposphere than gravity with periods shorter than 60 min.~~

Based on the development of both horizontal wind directions it holds for the last third of January: the later in January, the smaller the difference between the frequency and the intrinsic frequency is. If the intrinsic frequency is approximately equal to the ground-based frequency, then the vertical wavelength does not vary much with height (only due to the changing (angular) BV frequency). If we assume that wave fronts of high- and medium frequency waves are oriented 0–45° to the vertical and if we take into account that our measurements address ca. 90 km height, then the possible tropospheric source must be ca. 90 km and more away from Kiruna.

~~We can argue that especially mountain waves (phase velocity equal to zero) generated near Kiruna had the best chance to reach the OH airglow layer around January 21st and from January 24th to 28th. During the other time periods, the horizontal wind speed became zero in extended height intervals (Fig. 14), which prohibits a vertical propagation (Fritts and Alexander, 2003). Indeed, we observed the highest occurrence rate of band like structures during flight 5 (January 28th) when the airplane flew most of the time over the mountain chain and passed the highest elevations of the flight route.~~

~~Generally, we can conclude that at the end of January the source of high- and medium frequency waves generated in the lower troposphere would be at a horizontal distance of ca. 90 km height and more from the measurement place. During this time, the wind profile is rather flat, so the intrinsic frequency is approximately equal to the ground based frequency and the vertical wavelength does not vary much with height (only due to the changing (angular) BV frequency). If we assume that wave fronts of high- and medium frequency waves are oriented 0–45° to the vertical and if we take into account that our measurements address ca. 90 km height, then the possible tropospheric source must be ca. 90 km and more away from Kiruna.~~

In order to find out more about the different kinds of ripples, which we probably observed in the two flights, we need information about horizontal wind and temperature between 80 km and 100 km. Airborne or comprehensive ground-based measurements of these parameters are not available. Therefore, we do not get precise information about the background wind and about convective and dynamical instability along the flight track. We can therefore neither clearly distinguish between small-scale maybe secondary gravity waves and instability features nor (in the case of instability) between different kinds of instability.

From the temporal development of the (angular) BV frequency based on TIMED-SABER measurements (fig. 5), we can at least conclude that overall the tendency of the OH-airglow layer height to develop static instability increased during the measurement period. ~~In the following, we try to use the airglow brightness maps to learn more about convective and dynamic instability in the two flights.~~

Since the measurements were taken in winter~~Since it is winter~~, the mesopause is located above the OH* layer at ca. 100 km height (e.g., Lübken and Von Zahn, 1991). Thus, as long as inversion layers do not exist, the ~~overall~~ vertical background temperature gradient is negative in the height range of the OH* layer. Static instability is therefore possible and independent of the existence of gravity waves.

In the following, we try to use the information about airglow brightness to learn more about convective and dynamic instability in the two flights. This argumentation only holds if the wavelengths in the range of ripples are instability features and if the airglow brightness variations (shown in Fig. 8a and 11a) are caused by gravity waves. We like to emphasize that we cannot prove these two conditions but our own (FAIM) data and also wind measurements at ALOMAR do not disagree with them. Concerning the airglow brightness variations, we can argue that the horizontal distance between the intensity maxima (compare Fig. 8a and 7 and Fig. 11a and 10) does not contradict the gravity wave possibility. Concerning the instability features, we have to check the background wind. As mentioned wind information for the flight is not available but mesopause wind measurements derived at ALOMAR are published (Stober et al., 2017). During flight 1 on January 14th ALOMAR was passed three times, flight 5 on January 28th took place south of ALOMAR. The zonal wind (after removal of tides and gravity wave contributions) is directed eastward on January 14th and 28th 2016 at ALOMAR. On January 14th, the meridional component is nearly zero at ca. 86 km height, on January 28th, it is positive (northward). Wavelength in the range of 15 km and less derived from airborne FAIM measurements move to the northeast (and/or southwest) during flight 1 (Fig. 9); for flight 5, a preferred quadrant of propagation cannot be identified, however, a maximum is observed for a strict eastward (westward) propagation. So, we can at least say that the horizontal background wind at ALOMAR is not oriented perpendicular to the wave (ripple) propagation direction.

After having discussed the assumptions, we now come back to the actual argumentation. ~~However, i~~If gravity waves are present, then the probability for convective instability should change most in the grey regions of an airglow image (i.e., in the regions of average intensity) since the wave-induced absolute temperature gradient is maximal there. This can be explained as follows.

The brightness of the OH* layer is mainly determined by the availability of atomic oxygen, which is generated higher up in the atmosphere (Shepherd et al., 2006). All processes which lead to a vertical transport of atomic oxygen therefore influence this parameter. Thus, downward transport processes are more pronounced in brighter areas of OH-airglow images compared to darker ones.

If the vertical transport processes happen adiabatically, e.g. due to a wave, adiabatic warming, i.e., positive temperature deviations from the atmospheric background, should be observed in the brighter parts of an airglow image. Darker airglow regions should then be affected by negative temperature deviations from the atmospheric background. Grey regions should

Formatiert: Nicht Hervorheben
Formatiert: Nicht Hervorheben
Formatiert: Nicht Hervorheben
Formatiert: Nicht Hervorheben
Formatiert: Nicht Hervorheben
Formatiert: Nicht Hervorheben
Formatiert: Hochgestellt
Formatiert: Hochgestellt
Formatiert: Hochgestellt
Formatiert: Hochgestellt
Formatiert: Hochgestellt
Formatiert: Hochgestellt

be characterized by nearly no temperature deviation from the atmospheric background. We would like to emphasize here that a strict correlation between airglow brightness and temperature in the sense of the brighter the airglow, the higher the temperature and vice versa does not hold as for example Fig. 7 of Pautet et al. (2014) makes clear. However, at least during this time of the year this assumption holds on average (Garcia-Comas et al., 2017; Shepherd et al., 2006). So, if the vertical movements of atomic oxygen are due to a wave, one can conclude that the wave-induced vertical temperature gradient becomes zero where the brightness is maximal or minimal, while the grey regions can be interpreted as the zero-crossings of a wave observed in a vertical temperature profile. There, the steepest absolute vertical temperature gradient exists and the static stability of the atmosphere is most influenced. ~~It can be higher or lower compared to the regions between the zero-crossings.~~

The probability for dynamic instability should change most in the bright and dark regions of an airglow image. This follows from the gravity wave polarization equations: the zonal wind shear is maximized when the temperature is extreme (Heale et al., 2017).

As mentioned in the previous section, pronounced wave activity, also in the range of small-scale wave-like structures, is observed in bright airglow areas during flight 1 (ca. 16:20–16:35 UTC, 17:30–18:00 UTC, 18:30–18:55 UTC). If we assume, that these small-scale structures are ripples in the sense of an instability feature and that the generating gravity waves dominate the averaged airglow images, then this observation means that the ripples are mainly due to dynamical instability. For flight 5, the situation is different. Here, pronounced wave activity also of small-scale wave-like structures is not necessarily linked to very bright airglow areas. For example, at the beginning of our measurements, relatively low wave activity can be observed while the airglow brightness shows a broad maximum (Fig. 11). It is followed by a period (around 18:40 UTC–18:45 UTC) during which the airglow brightness is neither maximal nor minimal but relatively high wave activity is present. Therefore, our observations are consistent with the assumption that~~we conclude that~~ overall the importance of dynamical instability is smaller for this flight compared to the first one. However, as Li at al. (2017) point out the percentage of ripples which advect with background winds is ~30% in both summer and winter in their data basis, which is probably the largest one investigated with respect to this phenomenon. This number is much lower than expected. Therefore, the probability is high that also in our case a large part of the observed ripples are not instability features.

Formatiert: Englisch (USA)

6 Summary and conclusion

Wave-like structures in the range of ripples and bands, ca. 3–25 km horizontal wavelength, were observed during two selected flights (flight 1 on January, 14th, 2016 and flight 5 on January, 28th, 2016) of the airborne airglow camera FAIM in Northern Scandinavia. The flights were separated by 14 days and took place under different atmospheric conditions: while the stratospheric jet was rather strong during the first flight, it was much weaker during the last one. In the same time, ground-based airglow observations (temperature and intensity) as well as TIMED-SABER based measurements (OH-airglow layer height and thickness) revealed typical features of a stratospheric warming.

The activity of these wave-like structures depended on place and time. Regions of vanishing wave activity ~~could not be~~were not observed. The most mountainous regions were characterized by the highest occurrence rate of wave-like structures in both flights. For flight 1, this result is due to a large portion of structures in the range of ripples. At the time of this flight, the propagation of mountain waves was not possible or at least strongly reduced. This is probably not the case for flight 5.

~~We found hints for a higher probability of convectively-induced ripples in flight 5 compared to flight 1. This agrees with our observations of t~~The static stability of the airglow-layer height decreased during January based on TIMED-SABER. If one interprets ripples as instability features, the~~We found hints for a higher probability of convectively-induced ripples in flight 5 compared to flight 1. This agrees with our observations of t~~ investigation of the airborne FAIM data shows consistent results .

The wave potential energy referring to waves of ca. 25 km horizontal wavelength and more varied also in time (time period: 14th–30th January) as ground-based airglow observations by GRIPS combined with SABER data during January 2016 showed. For waves with periods longer than 60 min, it is characterized by signatures which would be expected for waves generated ~~below~~ in the tropospher~~ic jet~~e. ~~This does not hold for waves with p~~Periods shorter than 60 min evolve differently. Therefore, we conclude that wave events with periods longer than 60 min are generated at different heights than ~~might mainly be generated in the troposphere, while the source of~~ waves with periods shorter than 60 min. ~~might mainly be at the height or above the height of the stratospheric jet.~~

Formatiert: Nicht Hervorheben

Formatiert: Nicht Hervorheben

Formatiert: Hervorheben

Author contribution

Carsten Schmidt, Patrick Hannawald and Sabine Wüst assured the operability of the ground-based and airborne instruments, GRIPS and FAIM, during the GW-LCYCLE campaign. Martin G. Mlynczak and James M. Russell are responsible for the TIMED-SABER data. Patrick Hannawald, Sabine Wüst and Carsten Schmidt analyzed the data. Sabine Wüst and Michael Bittner formulated the respective research goals in the proposal GW-LCYCLE. Sabine Wüst wrote the manuscript and discussed it especially with Michael Bittner, Patrick Hannawald and Carsten Schmidt.

Competing Interests

The authors declare that they have no conflict of interest.

Acknowledgement

For the overall organization of the flight campaign, we thank our colleagues from DLR, especially Markus Rapp and Andreas Dörnbrack, institute of atmospheric physics (IPA). For the acquisition of the project GW-LCYCLE, we thank Markus Rapp. Verena Wendt and Jeng-Hwa Yee deserve gratitude for her preparatory work concerning the SABER data analysis.

We thank the German Ministry for Education and Research (BMBF, Grant agreement No: 01LG1206A) for funding. Some algorithms applied in this study were developed in the VAO-project LUDWIG which was funded by the Bavarian State Ministry for the Environment and Consumer Protection (project number TUS01 UFS-67093).

Processing and long-term archiving of the FAIM and GRIPS data is provided by the World Data Center for Remote Sensing of the Atmosphere (WDC-RSAT, http://wdc.dlr.de). The measurements are part of the Network for the Detection of Mesospheric Change, NDMC (https://www.wdc.dlr.de/ndmc).

References

Baker, D.J., Stair Jr., A.T., 1988. Rocket measurements of the altitude distributions of the hydroxyl airglow. Phys. Scripta 37, 611–622.

Clairemidi, J., Herse, M., and Moreels, G.: Bi-dimensional observations of waves near the mesopause at auroral latitudes, Planet. Space Sci., 33, 1013–1022, 1985.

Dawkins, E. C. M., Feofilov, A., Rezac, L., Kutepov, A. A., Janches, D., Höffner, J., Chu. X., Lu, X., Mlynczak, M. G., and J. Russell III; Validation of SABER v2.0 operational temperature data with ground-based lidars in the mesosphere-lower thermosphere region (75–105 km). J. Geophys. Res.: Atmos., 123, 9916–9934. 10.1029/2018JD028742, 2018.

Dunkerton, T. J., and Butchart, N.: Propagation and selective transmission of internal gravity waves in a sudden warming. J. Atmos. Sci., 41(8), 1443–1460, 1984.

Dörnbrack, A., Gisinger, S., Kaifler, N., Portele, T., Bramberger, M., Rapp, M., Gerding, M., Söder, J., Žagar, N., and Jelić, D.: Gravity Waves excited during a Minor Sudden Stratospheric Warming, Atmos. Chem. Phys. Discuss., 10.5194/acp-2018-228, in review, 2018.

Ern, M., Trinh, Q. T., Kaufmann, M., Krisch, I., Preusse, P., Ungermann, J., Zhu, Y., Gille, J. C., Mlynczak, M. G., Russell III, J. M., Schwartz, M. J., and Riese M.: Satellite observations of middle atmosphere gravity wave absolute momentum flux and of its vertical gradient during recent stratospheric warmings. Atmos. Chem. Phys., 16, 9983−10019, doi: 10.5194/acp-16-9983-2016, 2016.

France, J. A., Harvey, V. L., Alexander, M. J., Randall, C. E., and Gille, J. C.: High Resolution Dynamics Limb Sounder observations of the gravity wave-driven elevated stratopause in 2006. J. Geophys. Res., 117, D20108, doi: 10.1029/2012JD017958, 2012.

Fritts, D. C., J. R. Isler, J. H. Hecht, R. L. Walterscheid, and Andreassen, O.: Wave breaking signatures in sodium densities and OH nightglow. 2. Simulation of wave and instability structures, J. Geophys. Res., 102, 6669–6684, doi:10.1029/96JD01902, 1997.

Fritts, D. C., and Alexander, M. J.: Gravity wave dynamics and effects in the middle atmosphere, Rev. Geophys., 41, 1003, doi: 10.1029/2001RG000106, 2003.

García-Comas, M., López-Puertas, M., Marshall, B. T., Wintersteiner, P. P., Funke, B., Bermejo-Pantaleón, D. Mertens, C. J., Remsberg, E. E., Gordley, L. L., Mlynczak, M. G., and Russell III, J. M.. Errors in Sounding of the Atmosphere using Broadband Radiometry (SABER) kinetic temperature caused by non-local-thermodynamic-equilibrium model parameters. J. Geophys. Res., 113, D24106. 10.1029/2008JD010105, 2008.

García-Comas, M., López-González, M. J., González-Galindo, F., Rosa, J. L. D. L., López-Puertas, M., Shepherd, M. G., and Shepherd, G. G.: Mesospheric OH layer altitude at midlatitudes: Variability over the Sierra Nevada Observatory in Granada, Spain (37°N, 3°W), Ann. Geophys., 35, 1151–1164, 10.5194/angeo-35-1151-2017, 2017.

Grygalashvyly, M.: Several notes on the OH layer, Ann. Geophys., 33, 923–930, 10.5194/angeo-33-923-2015, 2015.

Formatiert: Englisch (Großbritannien)
Formatiert: Englisch (USA)
Formatiert: Englisch (USA)
Formatiert: Englisch (USA)
Formatiert: Englisch (USA)
Formatiert: Absatz-Standardschriftart
Formatiert: Englisch (Großbritannien)
Formatiert: Englisch (Großbritannien)
Formatiert: Englisch (Großbritannien)
Formatiert: Englisch (Großbritannien)
Formatiert: Englisch (Großbritannien)
Formatiert: Englisch (Großbritannien)
Formatiert: Englisch (Großbritannien)
Formatiert: Englisch (Großbritannien)
Formatiert: Deutsch (Deutschland)
Formatiert: Deutsch (Deutschland)
Formatiert: Deutsch (Deutschland)
Formatiert: Deutsch (Deutschland)
Formatiert: Englisch (USA)
Formatiert: Englisch (USA)

Hannawald, P., Schmidt, C., Wüst, S., and Bittner, M.: A fast SWIR imager for observations of transient features in OH airglow, Atmos. Meas. Tech., 9, 1461–1472, doi:10.5194/amt-9-1461-2016, 2016.

Hannawald, P., Schmidt, C., Sedlak, R., Wüst, S., and Bittner, M.: Seasonal and intra-diurnal variability of small-scale gravity waves in OH airglow at two Alpine stations,- Atmos. Meas. Tech., 12, 457–469, doi: 10.5194/amt-12-457-2019, ~~submitted to AMT~~2019.

Heale, C. J., Bossert, K., Snively, J. B., Fritts, D. C, Pautet, P.-D. and Taylor, M. J.: Numerical modeling of a multiscale gravity wave event and its airglow signatures over Mount Cook, New Zealand, during the DEEPWAVE campaign, J. Geophys. Res. Atmos., 122, 846–860, doi:10.1002/2016JD025700, 2017.

Hecht, J. H.: Instability layers and airglow imaging. Rev. Geophys., 42(1), 2004.

Krassovsky, V.I., Shefov, N.N., and Yarin, V.I.: Atlas of the airglow spectrum 3000–12400 Å. Planet. Space Sci. 9, 883, doi: 10.1016/0032-0633(62)90008-9, 1962.

Li, T., She, C. Y., Williams, B. P., Yuan, T., Collins, R. L., Kieffaber, L. M., & Peterson, A. W.: Concurrent OH imager and sodium temperature/wind lidar observation of localized ripples over northern Colorado. J. Geophys. Res. Atmos., 110(D13), 2005.

Li, J., Li, T., Dou, X., Fang, X., Cao, B., She, C.-Y., Nakamura, T., Manson, A., Meek, C. and Thorsen, D.: Characteristics of ripple structures revealed in OH airglow images, J. Geophys. Res. Space Physics, 122, 3748–3759, doi: 10.1002/2016JA023538, 2017.

Liu, H. L.: Gravity Wave Variation from the Troposphere to the Lower Thermosphere during a Stratospheric Sudden Warming Event: A Case Study. SOLA, 13(Special Edition), 24-30, doi: 10.2151/sola.13A-005, 2017.

Liu, G. and Shepherd, G. G.: An empirical model for the altitude of the OH nightglow emission. Geophys. Res. Lett., 33(9), 2006.

López-Puertas, M., Garcia-Comas, M., Funke, B., Picard, R. H., Winick, J. R., Wintersteiner, P. P., Mlynczak, M. G., Mertens, C. J., Russell III, J. M., and Gordley, L. L.: Evidence for an OH (v) excitation mechanism of CO_2 4.3 μm nighttime emission from SABER/TIMED measurements, J. Geophys. Res., 109, D09307, doi: 10.1029/2003JD004383, 2004.

Lübken, F.-J., and von Zahn, U.: Thermal structure of the mesopause region at polar latitudes. J. Geophys. Res. Atmos., 96(D11):20841–20857, 1991.

Manney, G. L., and Lawrence, Z. D.: The major stratospheric final warming in 2016: dispersal of vortex air and termination of Arctic chemical ozone loss. Atmos. Chem. & Phys. 16.23, doi: 10.5194/acp-16-15371-2016, 2016.

Meinel, A.B., 1950. OH emission bands in the spectrum of the night sky. Part II. Astrophys. J. 112, 120–130.

Mies, F.H., 1974. Calculated vibrational transition probabilities of OH($X^2\Pi$). J. Mol. Spectrosc. 53 (2), 150–188, http://dx.doi.org/10.1016/0022-2852(74)90125-8.

Mertens, C. J., Schmidlin, F. J., Goldberg, R. A., Remsberg, E. E., Pesnell, W. D., Russell III, J. M., Mlynczak, M. G., López-Puertas, M., Wintersteiner, P. P., Picard, R. H., Winick, J. R., and Gordley, L. L.: SABER observations of

Formatiert: Englisch (USA)

Formatiert: Englisch (USA)

Formatiert: Englisch (USA)

mesospheric temperatures and comparisons with falling sphere measurements taken during the 2002 summer MaCWAVE campaign, Geophys. Res. Lett., 31, L03105, doi: 10.1029/2003GL018605, 2004.

Mertens, C. J., Fernandez, J. R., Xu, X., Evans, D. S., Mlynczak, M. G., and Russell III, J. M.: A new source of auroral infrared emission observed by TIMED/SABER, Geophys. Res. Lett., 35, 17–20, 2008.

Mlynczak, M. G.: Energetics of the mesosphere and lower thermosphere and the SABER experiment, Adv. Space Res., 20, 1177–1183, doi: 10.1016/S0273-1177(97)00769-2, 1997.

Mulligan, F. J., Dyrland, M. E., Sigernes, F., and Deehr, C. S.: Inferring hydroxyl layer peak heights from ground-based measurements of OH (6-2) band integrated emission rate at Longyearbyen (78°N, 16°E). Ann. Geophys., 27, 41974205, 2009.

O'Sullivan, D., and Dunkerton, T. J.: Generation of inertia gravity waves in a simulated life cycle of baroclinic instability. J. Atmos. Sci., 52: 3695−3716, doi: 10.1175/1520-0469(1995)052<3695:GOIWIA>2.0.CO;2, 1995.

Pautet, P.-D., Taylor, M. J., Pendleton, W. R., Zhao, Y., Yuan, T., Esplin, R., and McLain, D.: Advanced mesospheric temperature mapper for high-latitude airglow studies. Appl. Opt., 53(26), 5934–5943, 2014.

Pautet, P.-D., Taylor, M. J., Fritts, D. C., Bossert, K., Williams, B. P., Broutman, D., Ma, J., Eckermann, S. D. and Doyle, J. D.: Large-amplitude mesospheric response to an orographic wave generated over the Southern Ocean Auckland Islands (50.7°S) during the DEEPWAVE project, J. Geophys. Res. Atmos., 121, 1431–1441, doi: 10.1002/2015JD024336, 2016.

Remsberg, E. E., Marshall, B. T., Garcia-Comas, M., Krueger, D., Lingenfelser, G. S., Martin-Torres, J., Mlynczak, M. G., Russell III, J. M., Smith, A. K., Zhao, Y., Brown, C., Gordley, L. L., Lopez-Gonzalez, M. J., Lopez-Puertas, M., She, C.-Y., Taylor, M. J., and Thompson, R. E.: Assessment of the quality of the Version 1.07 temperature versus pressure profiles of the middle atmosphere from TIMED/SABER, J. Geophys. Res., 113, D17101, doi: 10.1029/2008JD010013, 2008.

Russell III, J. M., Mlynczak, M. G., Gordley, L. L., Tansock Jr., J. J., and Esplin, R. W.: Overview of the SABER experiment and preliminary calibration results, Proc. SPIE 3756, Optical Spectroscopic Tech. Instrum. Atmos. Space Res. III, 277–288, doi: 10.1117/12.366382, 1999.

Schmidt, C., Höppner, K., Bittner, M.: A ground-based spectrometer equipped with an InGaAs array for routine observations of OH(3-1) rotational temperatures in the mesopause region, J. Atmos. Sol.-Terr. Phys., 102, 125–139, doi: 10.1016/j.jastp.2013.05.001, 2013.

Shepherd, G. G., Cho, Y.-M., Liu, G., Shepherd, M. G., and Roble, R. G.: Airglow variability in the context of the global mesospheric circulation. J. Atmos. Sol.-Terr. Phys. 68(17), 2000–2011, 2006.

Stober, G., Matthias, V., Jacobi, C., Wilhelm, S., Höffner, J., and Chau, J. L.: Exceptionally strong summer-like zonal wind reversal in the upper mesosphere during winter 2015/16. Ann. Geophys. 35 (3), 711–720), doi: 10.5194/angeo-35-711-2017, 2017.

Formatiert: Englisch (USA)

Formatiert: Englisch (USA)

Takahashi, H., Batista, P. P., Sahai, Y., and Clemesha, B. R.: Atmospheric wave propagations in the mesopause region observed by the OH (8, 3) band, NaD, O2A (8645Å) band and OI 5577 Å nightglow emissions. Planet. Space Sci., 33(4), 381–384, 1985.

Taylor, M. J., Bishop, M. B., and Taylor, V.: All-sky measurements of short period gravity waves imaged in the OI(557.7 nm), Na(589.2 nm) and near infrared OH and O2(0,1) nightglow emissions during the ALOHA-93 campaign, Geophys. Res. Lett., 22, 2833–2836, 1995.

Thurairajah, B., Bailey, S. M., Cullens, C. Y., Hervig, M. E. and Russell III, J. M.: Gravity wave activity during recent stratospheric sudden warming events from SOFIE temperature measurements. J. Geophys. Res., 119, 8091–8103, doi:10.1002/2014JD021763, 2014.

Vadas, S. L., Fritts, D. C., and Alexander, M. J.: Mechanism for the generation of secondary waves in wave breaking regions, J. Atmos. Sci., 60(1), 194–214, doi:10.1175/1520-0469(2003)060<0194:mftgos>2.0.co;2, 2003.

von Savigny, C.: Variability of OH(3-1) emission altitude from 2003 to 2011: Long-term stability and universality of the emission rate - altitude relationship, J. Atmos. Sol.-Terr. Physics, 127, 2015.

von Savigny, C., McDade, I. C., Eichmann, K. U., and Burrows, J. P.: On the dependence of the OH* Meinel emission altitude on vibrational level: SCIAMACHY observations and model simulations, Atmos. Chem. Phys., 12, 8813–8828, doi: 10.5194/acp-12-8813-2012, 2012.

Whiteway, J. A., and Carswell, A. I.: Rayleigh lidar observations of thermal structure and gravity wave activity in the high Arctic during a stratospheric warming. J. Atmos. Sci., 51(21), 3122–3136, 1994.

Wachter, P., Schmidt, C., Wüst, S., and Bittner, M.: Spatial gravity wave characteristics obtained from multiple OH(3-1) airglow temperature time series, J. Atmos. Sol.-Terr. Phys., 135, 192–201, doi: 10.1016/j.jastp.2015.11.008, 2015.

Wendt, V., Wüst, S., Mlynczak, M. G., Russell III, J. M., Yee, J.-H., and Bittner, M.: Impact of atmospheric variability on validation of satellite-based temperature measurements. J. Atmos. Sol.-Terr. Phys. 102: 252–260. DOI: 10.1016/j.jastp.2013.05.022, 2013.

Wright, C. J., Osprey, S. M., Barnett, J. J., Gray, L. J., and Gille, J. C.: High Resolution Dynamics Limb Sounder measurements of gravity wave activity in the 2006 Arctic stratosphere. J. Geophys. Res., 115, D02105, doi: 10.1029/2009JD011858, 2010.

Wüst, S., Wendt, V., Schmidt, C., Lichtenstern, S., Bittner, M., Yee, J.-H., Mlynczak, M. G., and Russell III, J. M.: Derivation of gravity wave potential energy density from NDMC measurements, J. Atmos. Sol.-Terr. Phys., 138, 32–46, doi: 10.1016/j.jastp.2015.12.003, 2016.

Wüst, S., Schmidt, C., Bittner, M., Silber, I., Price, C., Yee, J.-H., Mlynczak, M.G., and Russel III, J.M.: First ground-based observations of mesopause temperatures above the Eastern-Mediterranean Part II: OH*-climatology and gravity wave activity. J. Atmos. Sol Terr. Phys., 155, 104–111, doi: 10.1016/j.jastp.2017.01.003, 2017a.

Wüst, S., Bittner, M., Yee, J.-H., Mlynczak, M. G., and Russell III, J. M.: Variability of the Brunt-Väisälä frequency at the OH*-layer height, Atmos. Meas. Tech., 10, 4895–4903, doi: 10.5194/amt-10-4895-2017, 2017b.

Wüst, S., Wendt, V., Linz, R., and Bittner, M.: Smoothing data series by means of cubic splines: quality of approximation and introduction of a repeating spline approach. Atmos. Meas. Tech., 10, 3453–3462, doi: 10.5194/amt-10-3453-2017, 2017c.

Wüst, S., Offenwanger, T., Schmidt, C., Bittner, M., Jacobi, C., Yee, J.-H., Mlynczak, M. G., and Russell III, J. M.: Derivation of gravity wave intrinsic parameters and vertical wavelength using a single scanning OH (3-1) airglow spectrometer. Atmos. Meas. Tech., 11, 2937–2947, doi: 10.5194/amt-11-2937-2018, 2018.

Yiğit E. and Medvedev, A.S.: Gravity waves in the thermosphere during a sudden stratospheric warming. Geophys Res Lett 39:L21101, 2012.

Yiğit, E., and Medvedev, A. S.: Role of gravity waves in vertical coupling during sudden stratospheric warmings. Geosci. Lett., 3(1), 27, doi: 10.1186/s40562-016-0056-1, 2016.

Zhang, F.: Generation of mesoscale gravity waves in upper tropospheric jet–front systems. J. Atmos. Sci., 61, 440−457, doi:10.1175/1520-0469(2004)061<0440:GOMGWI>2.0.CO;2, 2004.

Zhou, X., Holton, J. R., and Mullendore, G.L.: Forcing of secondary waves by breaking of gravity waves in the mesosphere, J. Geophys. Res., 107(D7), 4058, doi: 10.1029/2001JD001204, 2002.

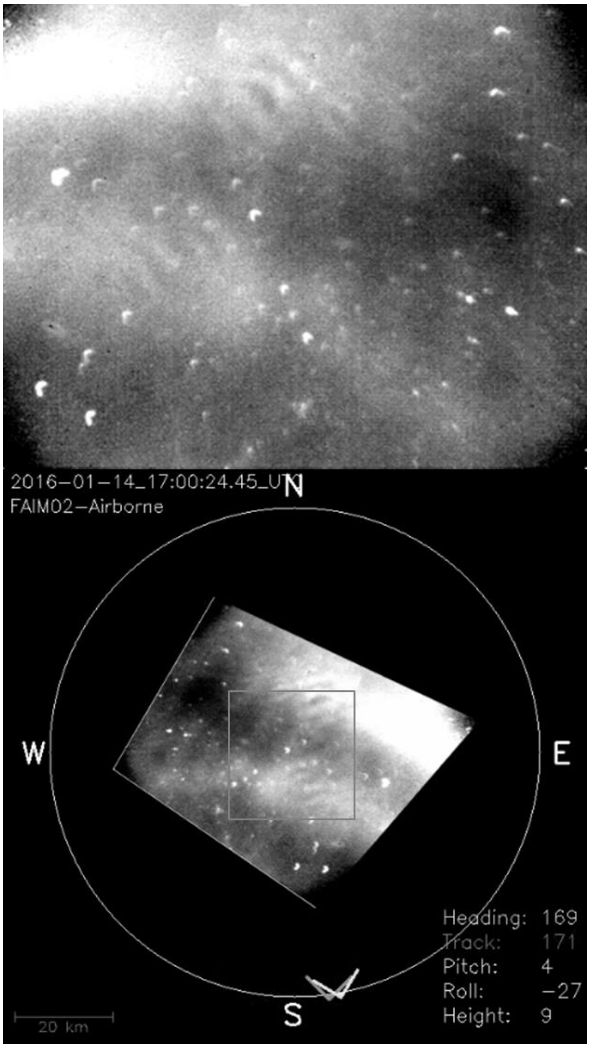
2016-01-14_17:00:24.45_UT
FAIM02-Airborne
N
W
E
S
Heading: 169
Track: 171
Pitch: 4
Roll: -27
Height: 9
20 km

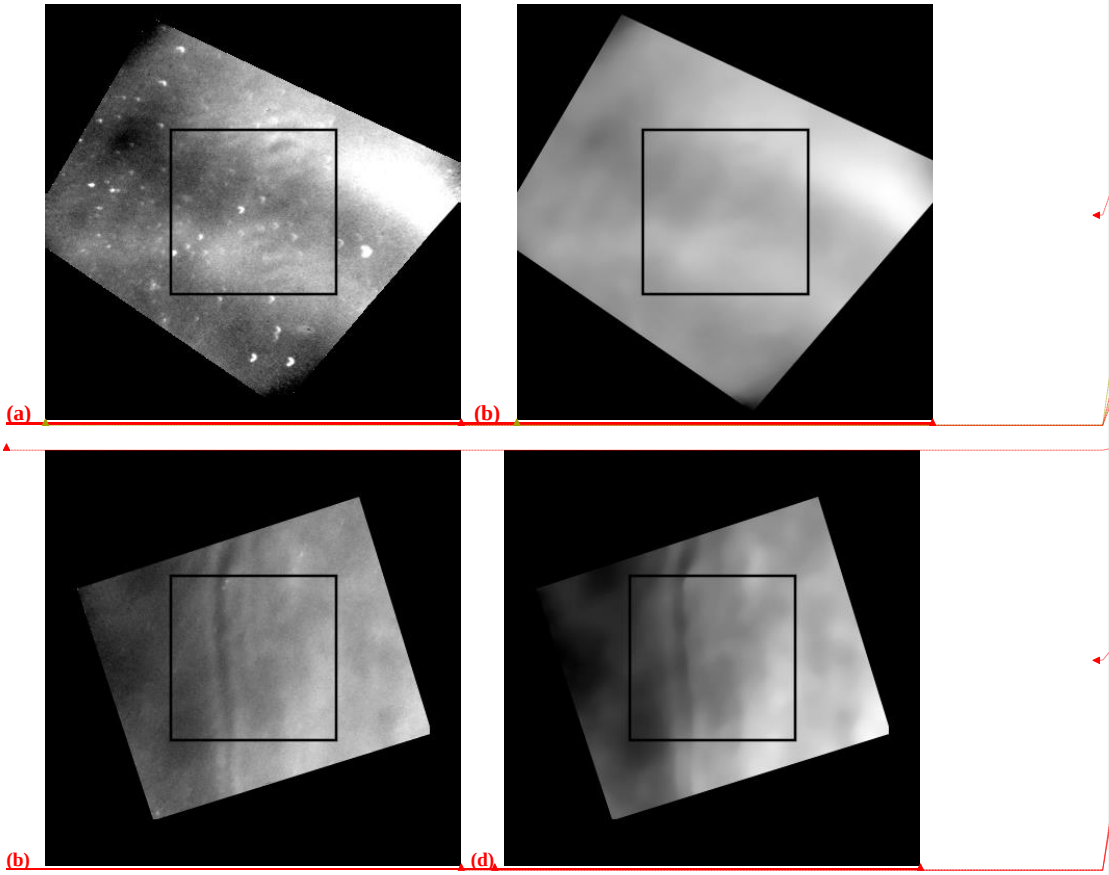

Figure 1: Images from the airborne FAIM 2 ~~imager~~ during the first flight. The ~~top~~ left ~~image~~ column (a and c) shows t~~w~~h~~o~~ ~~raw~~ images which are flat fielded ~~and~~, contrast adjusted~~. The bottom image shows the processed image with~~, ~~unwarping~~ un-warped (due to pitch, roll and yaw angle), rotated to a northward position and mirrored to fit the correct west-east position giving a satellite's view of the airglow layer. The right column (b and d) shows the same images after applying the median blur. ~~The square marks the region of interest which is used for calculation of the spectral analysis.~~ The image in the upper row (a and b) is an extreme example since the roll angle of -27° is rather high which results in a large image. For the analysis only absolute roll angles of 25° at maximum are used. This holds for the image shown in the second row (c and d). The squares mark the regions of interest which are used for the calculation of the spectral analysis if roll and pitch angles fulfil the selection criteria.

Formatiert: Schriftart: Fett

Formatiert: Listenabsatz, Nummerierte Liste + Ebene: 1 + Nummerierungsformatvorlage: a, b, c, … + Beginnen bei: 1 + Ausrichtung: Links + Ausgerichtet an: 0 cm + Einzug bei: 0,63 cm

Formatiert: Schriftart: Fett, Englisch (USA)

Formatiert: Schriftart: Fett

Formatiert: Schriftart: Fett, Englisch (USA)

Formatiert: Schriftart: Fett

Formatiert: Englisch (USA)

Formatiert: Englisch (USA)

Formatiert: Englisch (Großbritannien), Rechtschreibung und Grammatik prüfen

Formatiert: Nummerierte Liste + Ebene: 1 + Nummerierungsformatvorlage: a, b, c, … + Beginnen bei: 1 + Ausrichtung: Links + Ausgerichtet an: 0 cm + Einzug bei: 0,63 cm

Formatiert: Standard

~~(a)~~

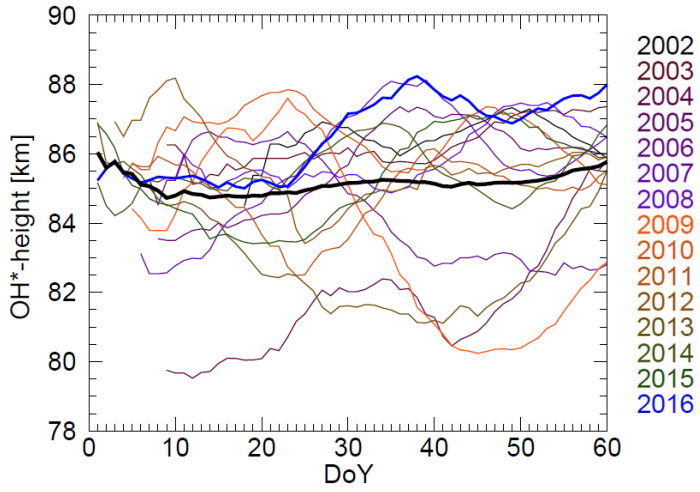
OH*-height [km]
DoY
2002
2003
2004
2005
2006
2007
2008
2009
2010
2011
2012
2013
2014
2015
2016

~~(b)~~

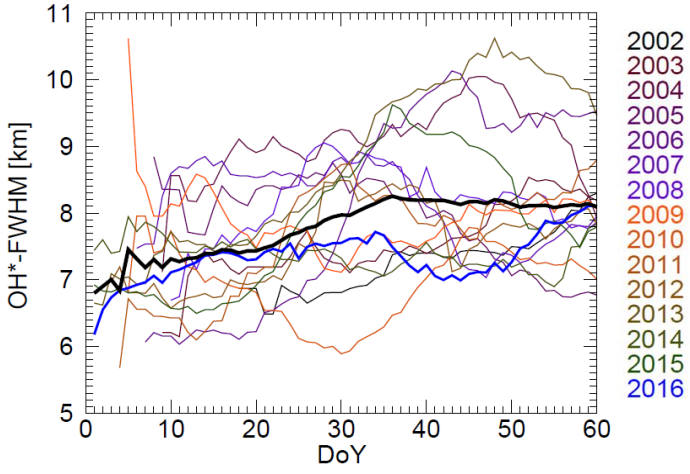
OH*-FWHM [km]
DoY
2002
2003
2004
2005
2006
2007
2008
2009
2010
2011
2012
2013
2014
2015
2016

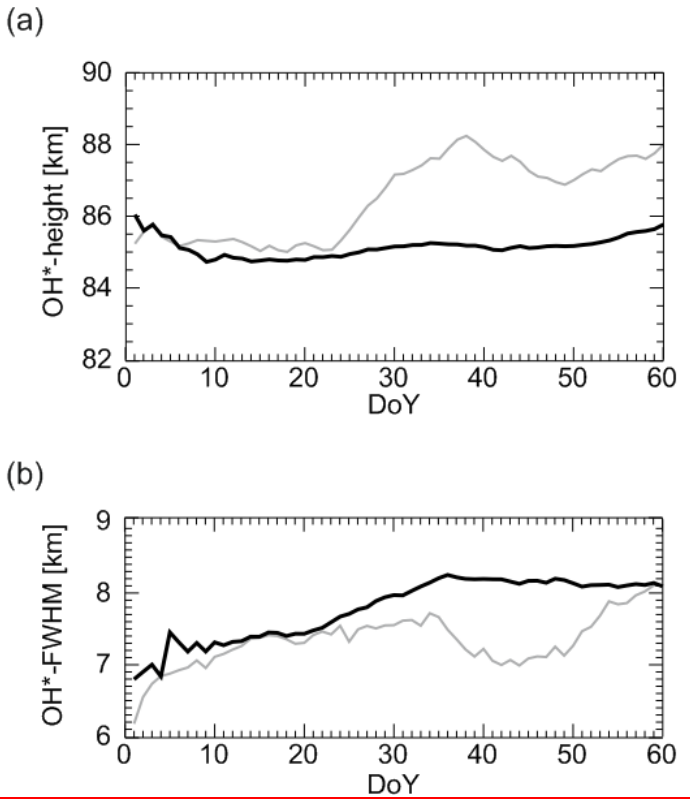

Figure 2: The different curves represent 15-days running means of the OH*-layer height (a) and its FWHM (b) calculated from TIMED-SABER ~~temperature~~ VER profiles (OH-B channel) within a rectangle centred at ALOMAR with 300 km edge length. Shown is the time period DoY 1-60. ~~for 2002–2016 (colour-coded, t~~The ~~bold~~ black line is the mean of all years, the ~~bold~~ greyblue line the year 2016~~).~~ If more than one value is available per day, a daily mean is calculated before smoothing. However, it can also happen that no SABER measurement is available for a specific day. ~~In this case, the smoothed value of all other valid points within the smoothing window is derived. Due to the yaw cycle of SABER, there is a larger data gap of some 10 days at the end of each year which can also affect the beginning of the subsequent year. This can limit the reliability of the smoothed data at the beginning of the individual years (see e.g. 2009). For 2015, data are available until day 312, in 2016 the time period DoY 5–65 is covered. Therefore, the results are reliable from day 12 until day 58 approximately.~~

(a)

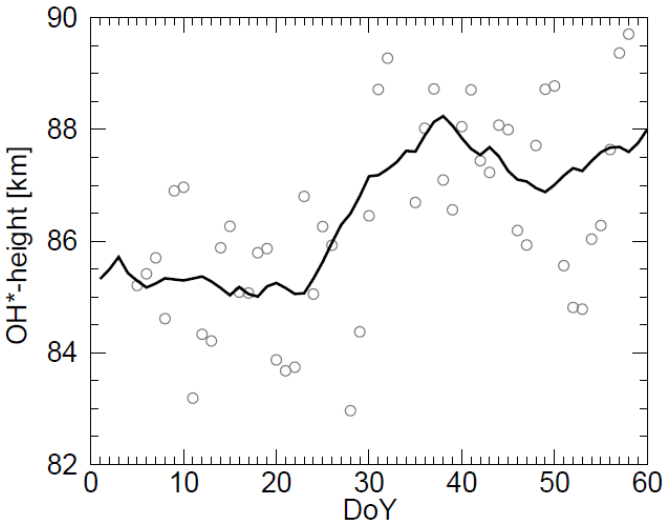

(b)

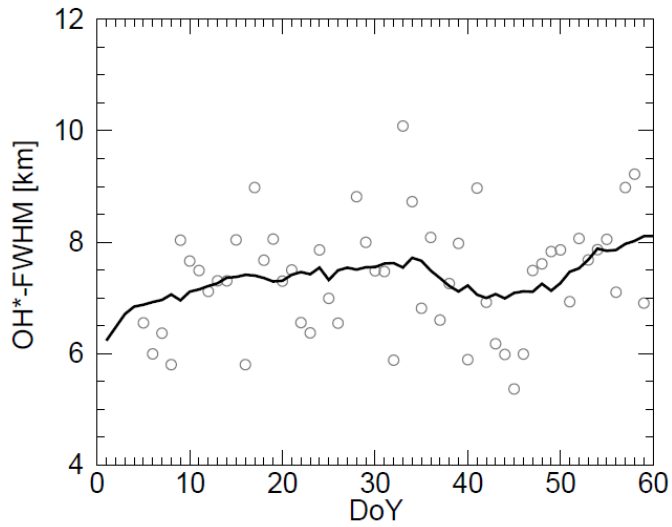

Figure 3: As in Figure 2~~Figure 2~~, the solid lines represent 15-days running means of the OH*-layer height (a) and its FWHM (b). The circles stand for the individual values. Shown is the year 2016.

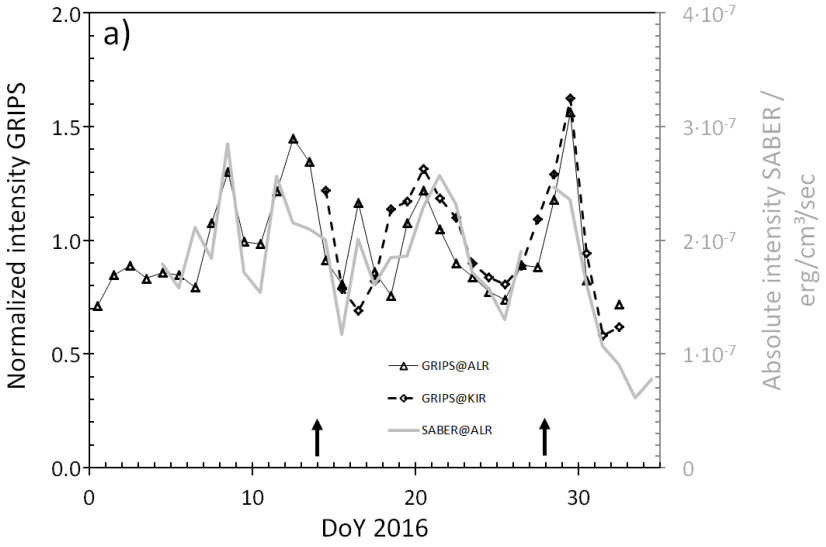
a)
Normalized intensity GRIPS
Absolute intensity SABER / erg/cm³/sec
DoY 2016
GRIPS@ALR
GRIPS@KIR
SABER@ALR
2.0
1.5
1.0
0.5
0.0
4·10⁻⁷
3·10⁻⁷
2·10⁻⁷
1·10⁻⁷
0
0
10
20
30

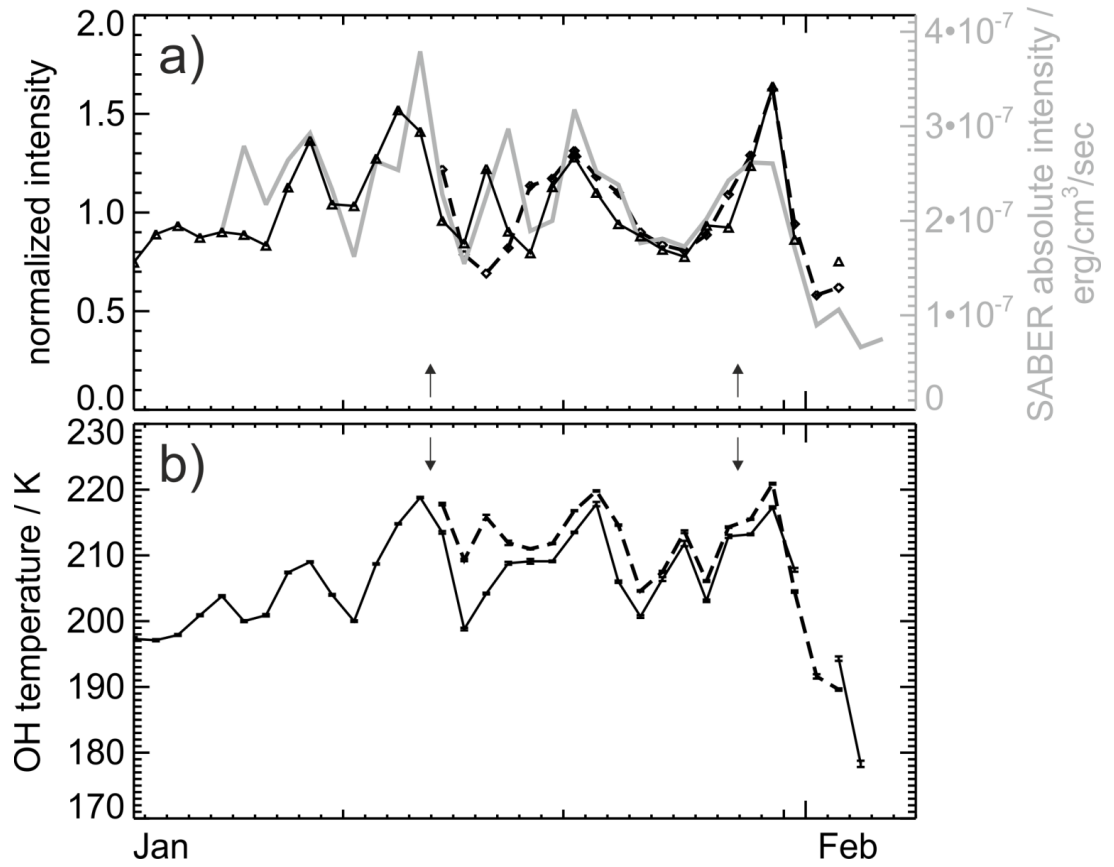
a)
b)
normalized intensity
SABER absolute intensity / erg/cm³/sec
OH temperature / K
2.0
1.5
1.0
0.5
0.0
4•10⁻⁷
3•10⁻⁷
2•10⁻⁷
1•10⁻⁷
0
230
220
210
200
190
180
170
Jan
Feb

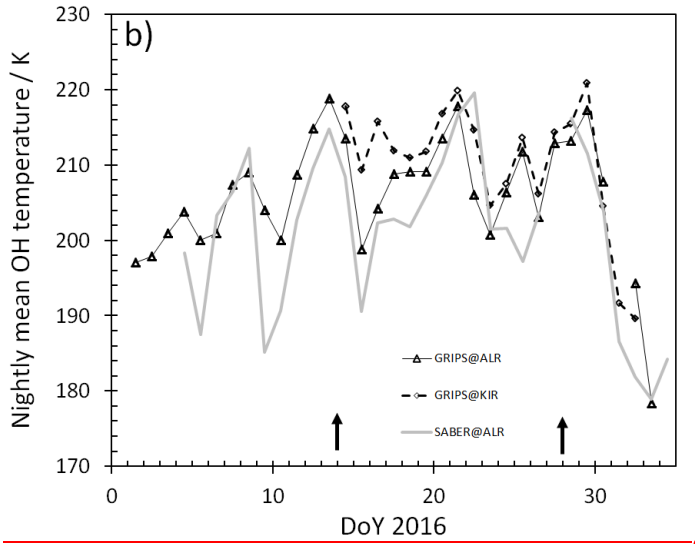

Figure 4: a) Average airglow intensity during the GW-LCYCLE campaign, covered by the three instruments GRIPS 14 at ALOMAR (solid, triangles), GRIPS 9 at Kiruna (dashed, diamonds) and SABER (grey) normalized to the respective mean intensity of the time period (1st of January to 3rd February 2016). The arrows mark the dates of flight 1 and 5. b) Nightly mean OH temperatures at ALOMAR (solid) and Kiruna (dashed). The ~~absolute~~ temperature values agree within ~~11~~ ca. 6 K ~~at maximum~~on average. This is one order of magnitude lower than ~~in the order of magnitude which can be~~ expected for this latitude, distance, and season ~~(see~~according to figure 5 from Wendt et al., ~~(~~2013 ~~for comparison))~~.

Formatiert: Englisch (USA)

Formatiert: Hochgestellt

Formatiert: Hochgestellt

Formatiert: Beschriftung

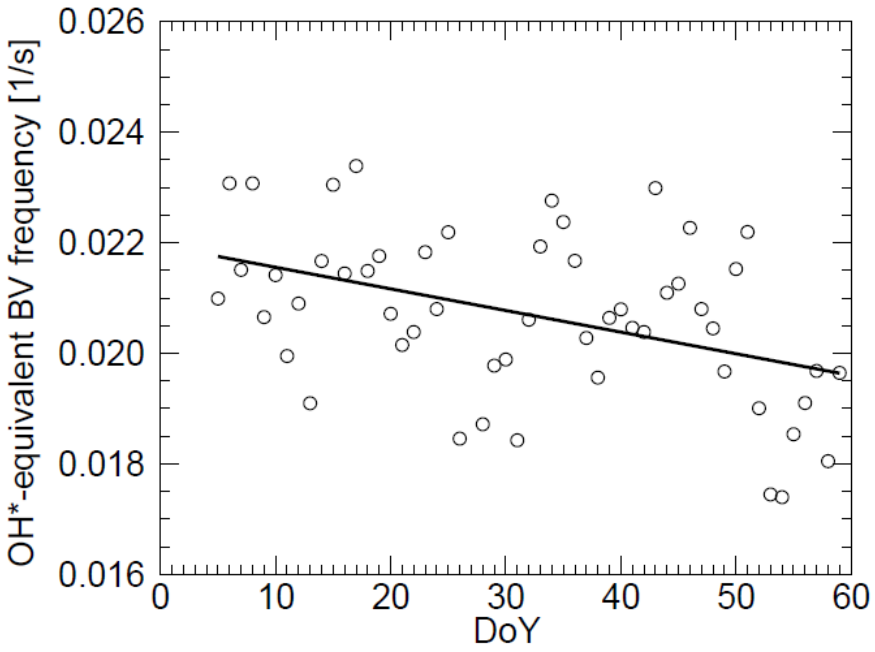

Figure 5: Overall, the OH*-equivalent (angular) Brunt-Väisälä (BV) frequency (circles are individual values) derived from SABER decreases from DoY 1–60 2016 over ALOMAR. The mean difference between the linear fit and the daily OH*-equivalent (angular) Brunt-Väisälä (BV) frequency is ca. 5%.

(a)

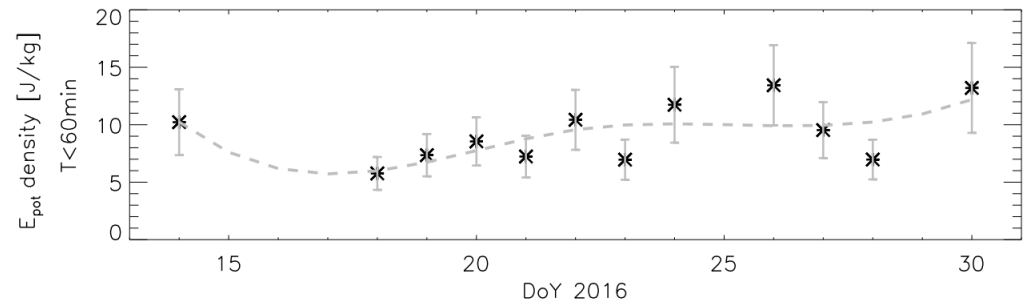

(b)

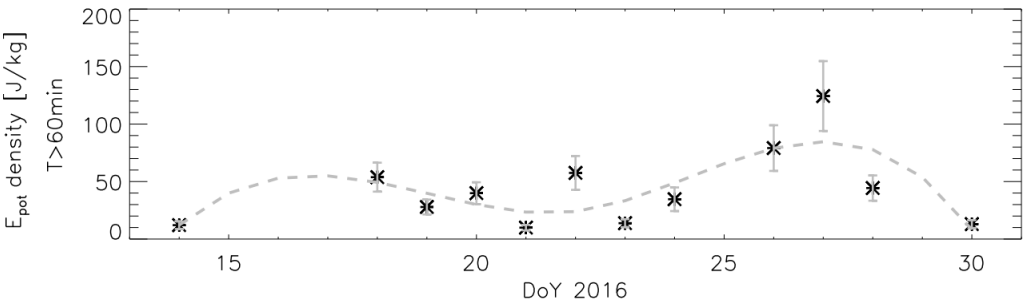

Figure 6 The upper plot shows the nightly mean wave potential energy density (based on GRIPS 9 measurements at Kiruna) for periods shorter than 60 min, while part b refers to periods longer than 60 min. The nightly mean OH*-equivalent (angular) BV frequency was taken from SABER. For the night from January 27th to 28th, coincident SABER profiles were not available, therefore, the mean based on the values of the night before and after was calculated. A cubic spline approximation is superimposed (dashed line).

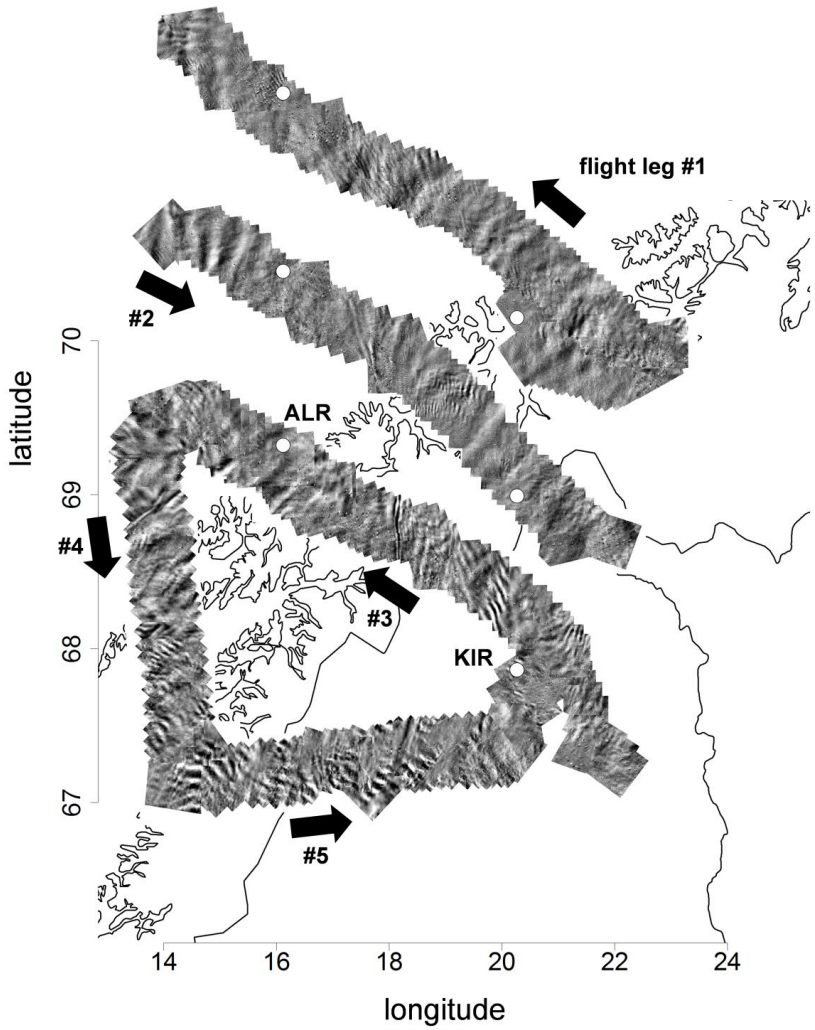

Figure 7: Difference images of the first flight (Jan 14). **A difference image is derived by subtracting the intensity measured by each pixel from the intensity measured 10 s later by the same pixel. The velocity of the airplane is approximately 210 m/s. So, the airplane moves ca. 2 km in 10 s. Calculating a difference image emphasizes horizontal structures which change significantly within 2 km and/or within 10 s in flight direction.** **Please note that the first three legs cover the same area, but legs one and two have been shifted for a better display.** **The black arrows show the flight direction.** **Apparently, the small scale structures change rapidly within a few minutes.**

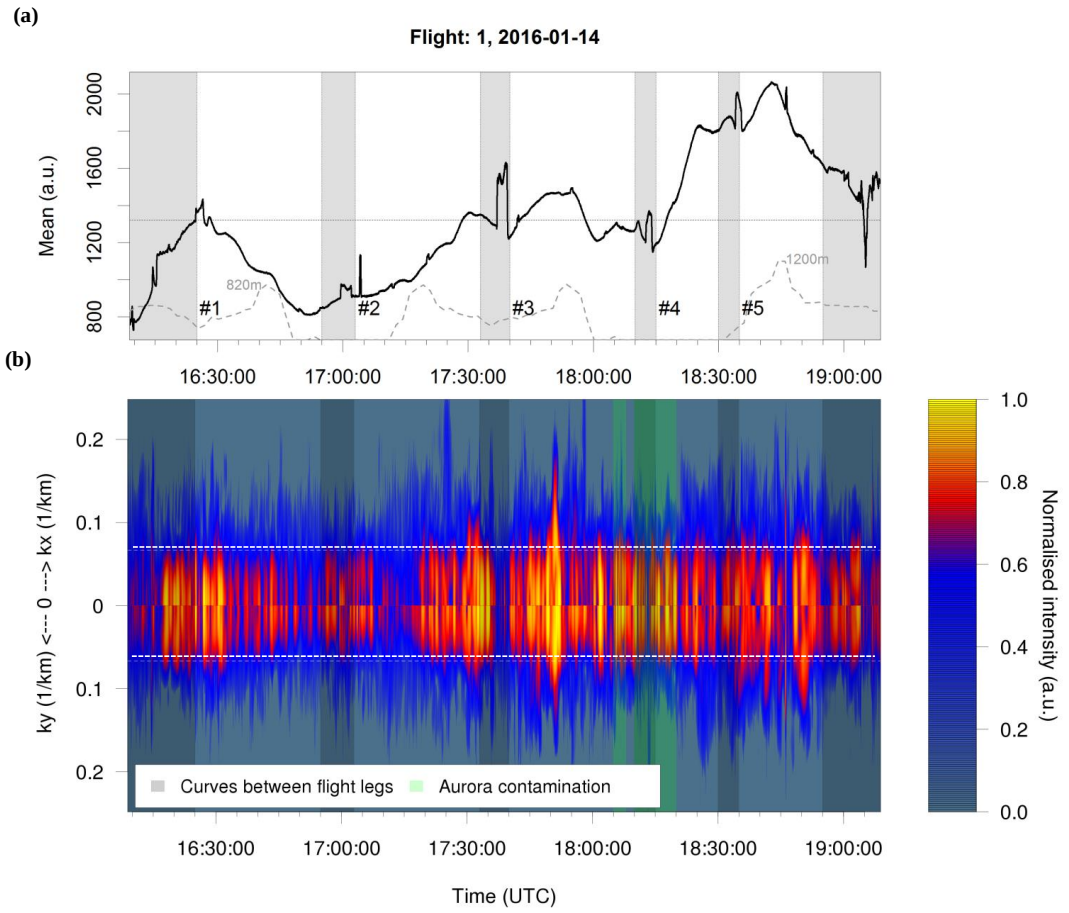

Figure 8 (a) Time series of integrated intensity per FAIM image. The grey areas refer to turning manoeuvres and should be excluded from further analysis. The grey line shows the orography. (b) 2D FFT spectra versus time: in the upper (lower) part the spectral intensity depends on the zonal (meridional) wave number. This plot is created by summing up the significant spectral

intensities over the meridional (zonal) wave numbers for each image. The colour bar is normalized in a way that the different spectra are comparable within one flight (logarithm to the basis of 10 is applied to each spectrum, mean and standard deviation over these values of the whole time series are calculated, values higher or lower than the mean plus or minus two times the standard deviation are set to 1 or 0). The horizontal line marks the wavelength of 15 km.

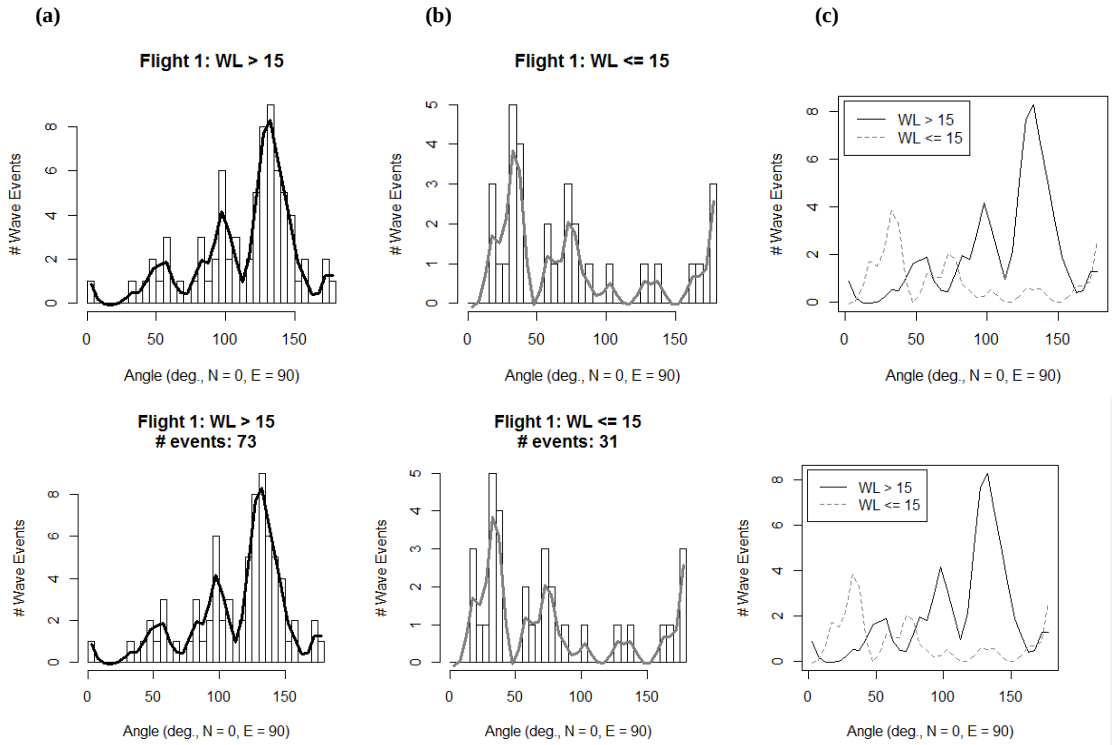

Figure 9 If wavelength and propagation direction are identical for at least six images separated by 30 s at maximum (parameter n), this wavelength is denoted as wave event. Wave events must be present for more than 10 s at least (time difference between first and last occurrence, parameter t). a) and b) depict the histograms of propagation directions (180° ambiguity, 5° bar width) smoothed by a cubic spline for wave events with horizontal wavelengths longer and shorter than 15 km for flight 1. Part c) shows both splines in one plot (black and grey: wavelength longer and shorter than 15 km). Smaller n and t change the absolute values for wavelengths longer than 15 km but not the qualitative results. Wavelengths shorter than 15 km are more sensitive to these parameters (especially to n) but with a stable peak at ca. 40°.

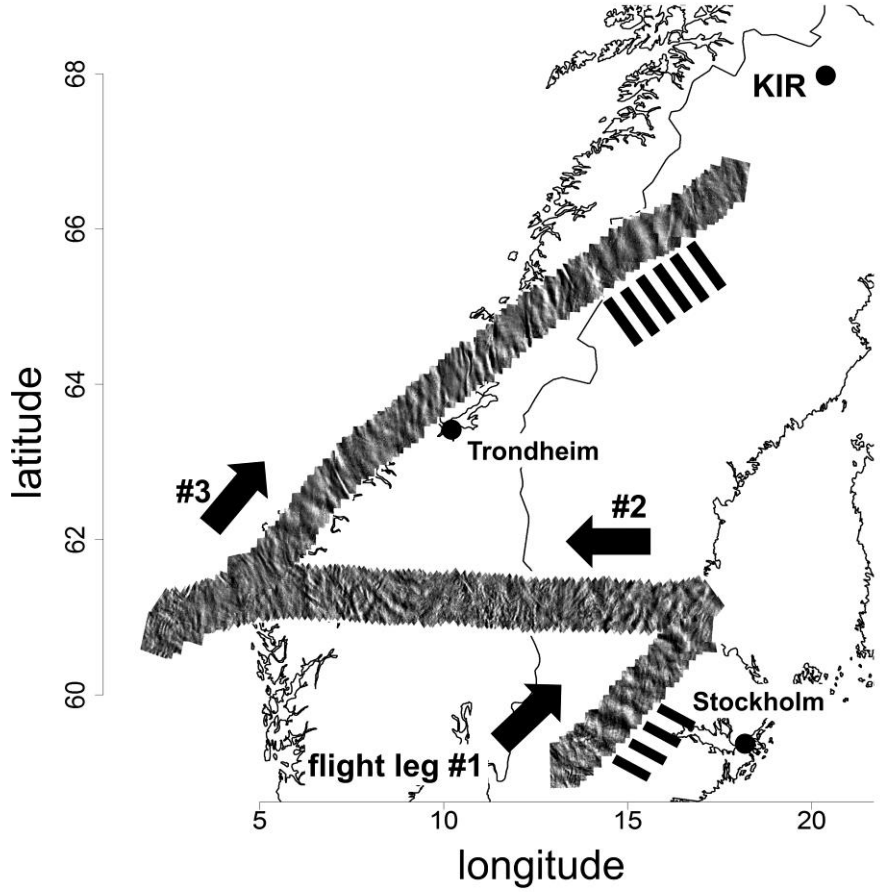

Figure 10: Same as Figure 7~~Figure 7~~ for the second flight of Jan 28, starting in Karlsbad. During the descent to Kiruna, high clouds obstructed the FoV and the respective observations are not shown. The black bars denote the appearance of gravity waves with larger scales than the instantaneous FoV.

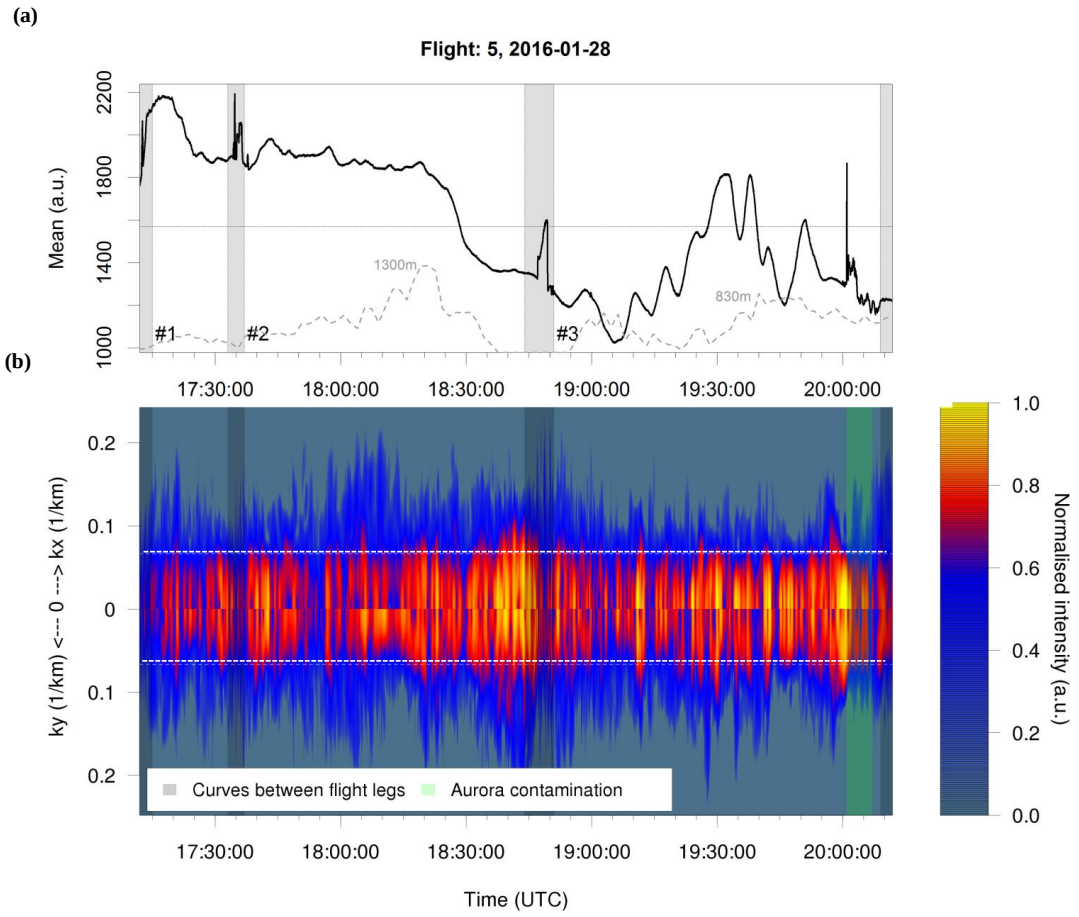

Figure 11 Same as Figure 8~~Figure 8~~ but for flight 5.

(a) **(b)** **(c)**

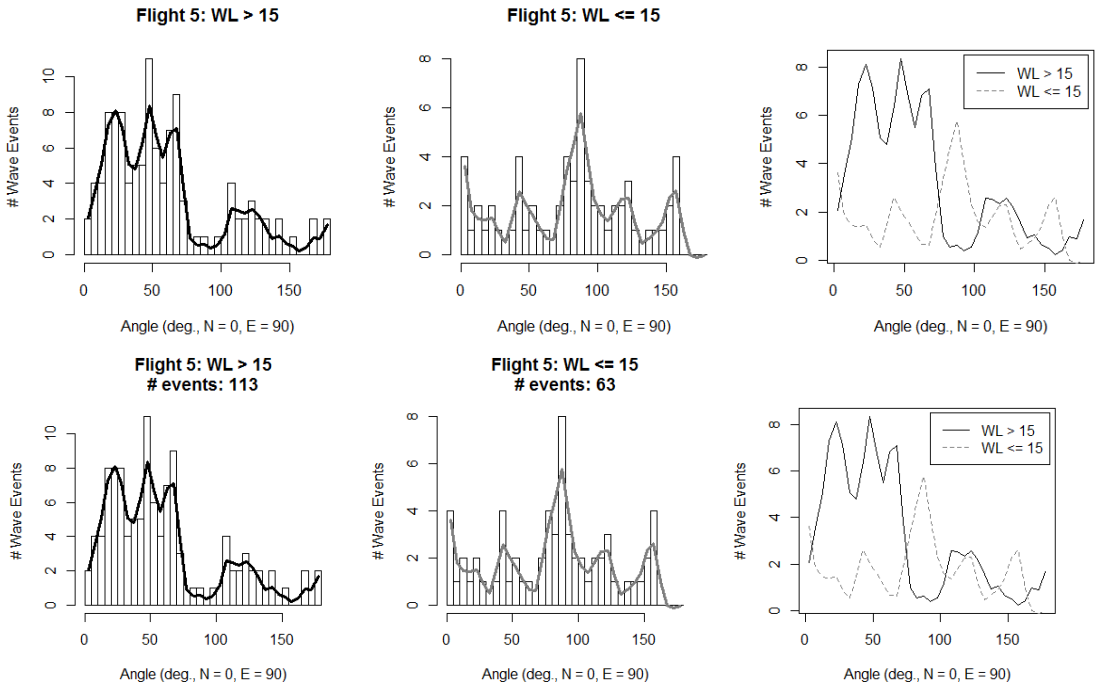
Flight 5: WL > 15
Wave Events
Angle (deg., N = 0, E = 90)
Flight 5: WL <= 15
Wave Events
Angle (deg., N = 0, E = 90)
WL > 15
WL <= 15
Wave Events
Angle (deg., N = 0, E = 90)
Flight 5: WL > 15
events: 113
Wave Events
Angle (deg., N = 0, E = 90)
Flight 5: WL <= 15
events: 63
Wave Events
Angle (deg., N = 0, E = 90)
WL > 15
WL <= 15
Wave Events
Angle (deg., N = 0, E = 90)

(d)

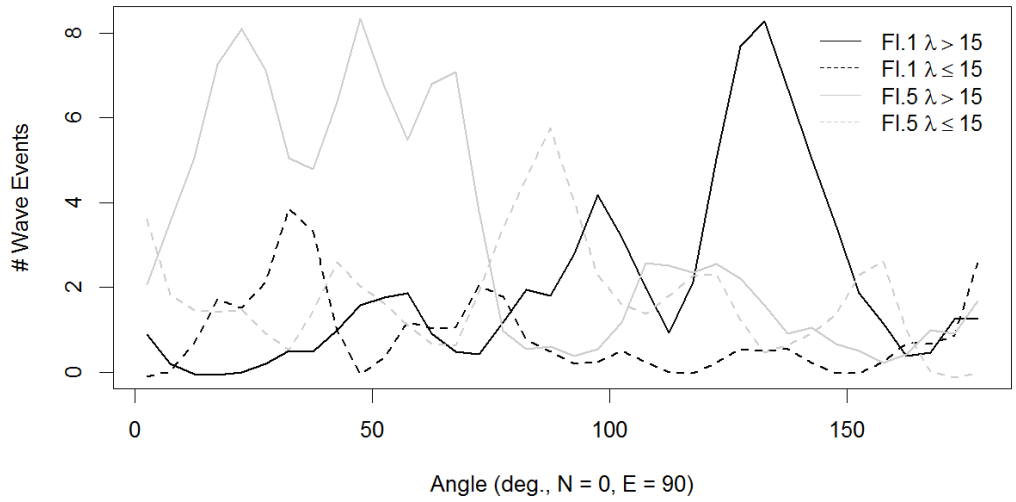

Figure 12 same as Figure 9~~Figure 9~~ but for flight 5. In this case, the results for both wavelength ranges are qualitatively stable for different n and t (the smaller n and t, the higher the absolute values). Part (d) shows the direct comparison of the results of both flights.

Formatiert: Standard

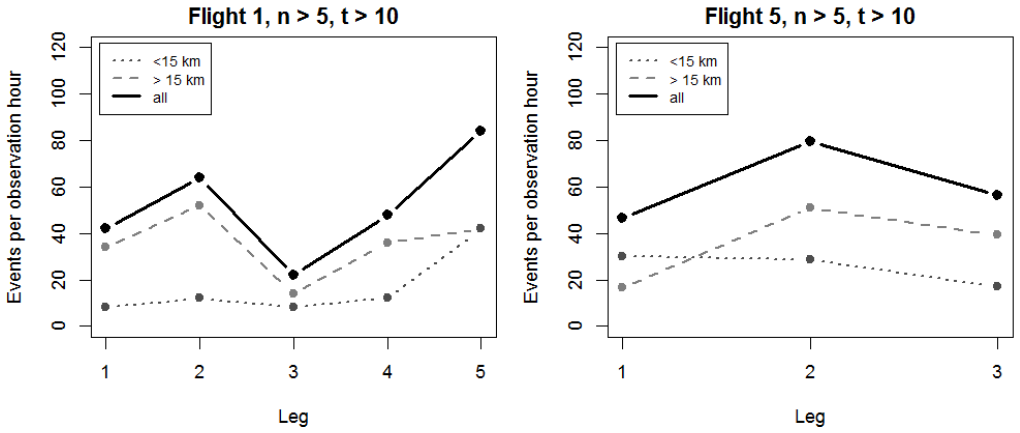

Figure 13 Occurrence rate of significant wave events for each leg of flight 1 and 5 (measurements during turning manoeuvres and aurora events are not included). The results are shown for wavelengths smaller (dotted line) and larger than 15 km (dashed line) as well as for the sum of both (solid line). If wavelength and propagation direction are identical for at least six images (parameter n) separated by 30 s at maximum, this wavelength is denoted as wave event. Wave events must be present for more than 10 s at least (time difference between first and last occurrence, parameter t). The results do not change qualitatively if n and t are smaller.

(a)

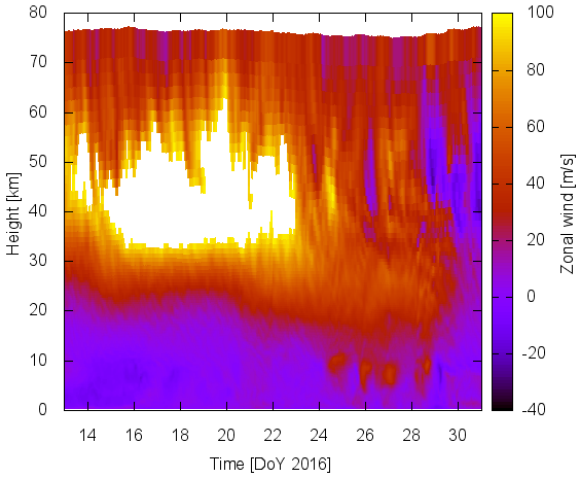
Height [km]
Time [DoY 2016]
Zonal wind [m/s]
80
70
60
50
40
30
20
10
0
14
16
18
20
22
24
26
28
30
100
80
60
40
20
0
-20
-40

(b)

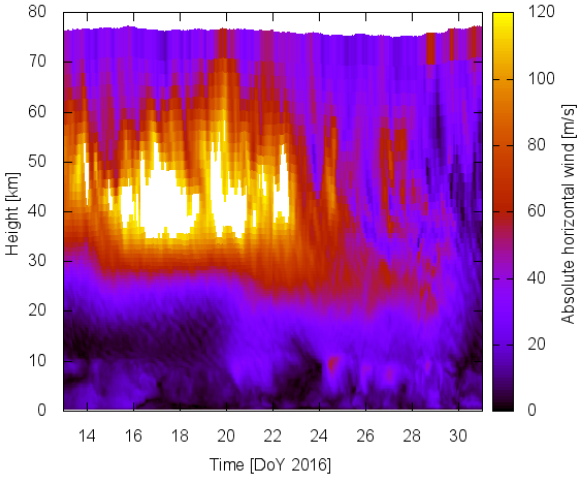
Height [km]
Time [DoY 2016]
Absolute horizontal wind [m/s]
80
70
60
50
40
30
20
10
0
14
16
18
20
22
24
26
28
30
120
100
80
60
40
20
0

(~~b~~c
)

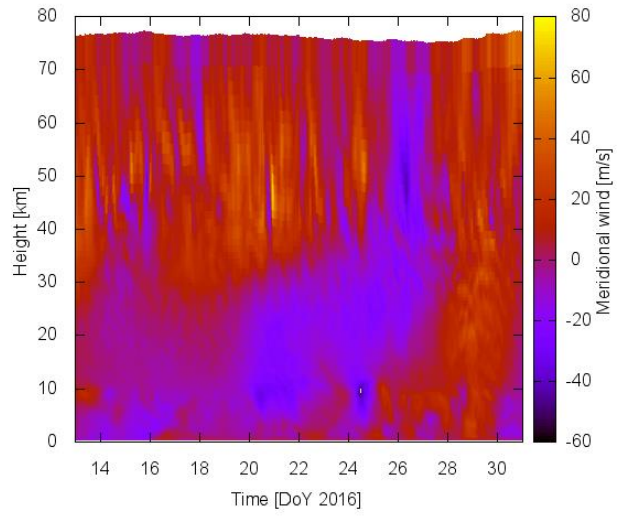

Figure 14 Zonal (a), ~~and~~ absolute horizontal (b), and meridional (c) wind at 67.84° N, 20.41° E (Kiruna: 67.86° N, 20.24° E) from ECMWF data (European Centre for Medium-Range Weather Forecast, ECMWF data were provided by Andreas Dörnbrack, DLR).